Intraventricular B7-H3 CAR T Cells for Diffuse Intrinsic Pontine Glioma: Preliminary First-in-Human Bioactivity and Safety

Nicholas A. Vitanza[1,2], Ashley L. Wilson[3], Wenjun Huang[3], Kristy Seidel[3], Christopher Brown[3,4], Joshua A. Gustafson[3], Jason K. Yokoyama[3], Adam J. Johnson[3], Blake A. Baxter[3], Ryan W. Koning[3], Aquene N. Reid[3], Michael Meechan[1], Matthew C. Biery[1], Carrie Myers[1], Stephanie D. Rawlings-Rhea[3], Catherine M. Albert[1,2], Samuel R. Browd[5], Jason S. Hauptman[5], Amy Lee[5], Jeffrey G. Ojemann[5], Michael E. Berens[6], Matthew D. Dun[7,8], Jessica B. Foster[9,10], Erin E. Crotty[1,2], Sarah E.S. Leary[1,2], Bonnie L. Cole[11,12], Francisco A. Perez[13], Jason N. Wright[13], Rimas J. Orentas[1,2], Tony Chour[12,14], Evan W. Newell[12,14], Jeffrey R. Whiteaker[15], Lei Zhao[15], Amanda G. Paulovich[15], Navin Pinto[1,2], Juliane Gust[16,17], Rebecca A. Gardner[1,2,3], Michael C. Jensen[3], and Julie R. Park[1,2,3]

ABSTRACT Diffuse intrinsic pontine glioma (DIPG) remains a fatal brainstem tumor demanding innovative therapies. As B7-H3 (CD276) is expressed on central nervous system (CNS) tumors, we designed B7-H3–specific chimeric antigen receptor (CAR) T cells, confirmed their preclinical efficacy, and opened BrainChild-03 (NCT04185038), a first-in-human phase I trial administering repeated locoregional B7-H3 CAR T cells to children with recurrent/refractory CNS tumors and DIPG. Here, we report the results of the first three evaluable patients with DIPG (including two who enrolled after progression), who received 40 infusions with no dose-limiting toxicities. One patient had sustained clinical and radiographic improvement through 12 months on study. Patients exhibited correlative evidence of local immune activation and persistent cerebrospinal fluid (CSF) B7-H3 CAR T cells. Targeted mass spectrometry of CSF biospecimens revealed modulation of B7-H3 and critical immune analytes (CD14, CD163, CSF-1, CXCL13, and VCAM-1). Our data suggest the feasibility of repeated intracranial B7-H3 CAR T-cell dosing and that intracranial delivery may induce local immune activation.

SIGNIFICANCE: This is the first report of repeatedly dosed intracranial B7-H3 CAR T cells for patients with DIPG and includes preliminary tolerability, the detection of CAR T cells in the CSF, CSF cytokine elevations supporting locoregional immune activation, and the feasibility of serial mass spectrometry from both serum and CSF.

INTRODUCTION

Diffuse intrinsic pontine glioma (DIPG) remains a universally fatal brainstem tumor affecting ~300 children per year in the United States at a median age of 6 years, making it responsible for more than 20,000 years of life lost each year (1). Although ~85% of DIPG harbor mutations in H3K27M, leading to their reclassification as diffuse midline glioma (DMG) H3K27M-altered, all DIPG have dismal clinical outcomes and may exhibit specific morbidities due to anatomic location (2, 3). As standard therapies for DIPG have not evolved since the incorporation of focal radiation (2), new approaches are critical to improving quality of life and overall survival for these children. Chimeric antigen receptor (CAR) T cells have demonstrated clinical efficacy against hematopoietic malignancies (4), but the utility of CAR T cells against DIPG is only now being explored (5).

B7-H3 (CD276) is an immunoregulatory member of the B7 protein family that is nearly universally expressed on the surface of atypical teratoid rhabdoid tumor (ATRT), DIPG, DMG, medulloblastoma, and high-grade glioma (HGG; refs. 6–9). Based on phase I clinical trial experience using locoregional CAR T cells targeting either HER2 or EGFR to treat pediatric patients with nonpontine DMG and other central nervous system (CNS) tumors (NCT03500991 and NCT03638167; ref. 10), we sought to develop B7-H3–specific CAR T cells and develop a phase I clinical trial of locoregional B7-H3 CARs for children with recurrent/refractory CNS tumors including DIPG.

Here, we describe preclinical *in vitro* and *in vivo* efficacy of a medium length (M) spacer B7-H3 CAR, consistent with other reports of preclinical efficacy (9, 11–16), as well as the novel incorporation of a human dihydrofolate reductase (DHFR) mutein, endowing methotrexate resistance for in-process selection to obtain a purified population of lentivirally transduced B7-H3–specific CAR-expressing T cells. We describe preliminary data from the open, ongoing, phase I, single-institution clinical trial BrainChild-03, delivering locoregional B7-H3 CARs to children and young adults with recurrent or refractory CNS tumors and DIPG (NCT04185038). Although BrainChild-03 has three distinct arms (A: localized recurrent/refractory CNS tumors; B: metastatic recurrent/refractory CNS tumors), here we report findings from the planned interim analysis of arm C, which included patients with DIPG

[1]Ben Towne Center for Childhood Cancer Research, Seattle Children's Research Institute, Seattle, Washington. [2]Department of Pediatrics, Seattle Children's Hospital, University of Washington, Seattle, Washington. [3]Seattle Children's Therapeutics, Seattle, Washington. [4]Therapeutic Cell Production Core, Seattle Children's Research Institute, Seattle, Washington. [5]Division of Neurosurgery, Seattle Children's Hospital and Department of Neurological Surgery, University of Washington, Seattle, Washington. [6]Cancer and Cell Biology Division, The Translational Genomics Research Institute (TGen), Phoenix, Arizona. [7]School of Biomedical Sciences and Pharmacy, College of Health, Medicine and Wellbeing, Callaghan, Australia. [8]Precision Medicine Research Program, Hunter Medical Research Institute, New Lambton Heights, Australia. [9]Division of Oncology, Children's Hospital of Philadelphia, Philadelphia, Pennsylvania. [10]Department of Pediatrics, University of Pennsylvania Perelman School of Medicine, Philadelphia, Pennsylvania. [11]Department of Laboratories, Seattle Children's Hospital, Seattle, Washington. [12]Department of Laboratory Medicine and Pathology, University of Washington School of Medicine, Seattle, Washington. [13]Department of Radiology, Seattle Children's Hospital, Seattle, Washington. [14]Vaccine and Infectious Disease Division, Fred Hutchinson Cancer Research Center, Seattle, Washington. [15]Clinical Research Division, Fred Hutchinson Cancer Center, Seattle, Washington. [16]Center for Integrative Brain Research, Seattle Children's Research Institute, Seattle, Washington. [17]Division of Pediatric Neurology, Department of Neurology, University of Washington, Seattle, Washington.

Note: M.C. Jensen and J.R. Park share senior authorship of this article.

Corresponding Author: Nicholas A. Vitanza, Seattle Children's Research Institute, M/S JMB-8, 1900 9th Avenue, Seattle, WA 98101. Phone: 206-884-4084; E-mail: nicholas.vitanza@seattlechildrens.org

enrolled at any time following standard radiotherapy (including patients with disease progression and/or metastatic disease). The first three evaluable patients on this arm constitute the only cohort across our three open CNS CAR T-cell trials (NCT03500991, NCT03638167, and NCT04185038) that does not incorporate intrapatient dose escalation. Therefore, all administered doses were at dose level (DL) 1 (i.e., 1×10^7 cells). This design allowed for the determination of tolerability before opening intrapatient dose escalation regimens. Ultimately, we report preliminary feasibility, tolerability, and correlative data including serial cerebrospinal fluid (CSF) mass spectrometry from this initial cohort of patients with DIPG receiving repeated intracranial B7-H3 CARs.

RESULTS

MGA271 scFv Fused to a Medium Extracellular Spacer Constitutes a CAR with Potent Antitumor Activity

Considering the frequency of B7-H3 expression on CNS tumors (7, 9, 12, 15), our team developed B7-H3 CARs using scFv binders derived from the MGA271 (huBRCA84D) monoclonal antibody (ref. 17; Supplementary Fig. S1A). CAR expression levels were confirmed by scFv protein-L staining and Western blot for CD3ζ (Supplementary Fig. S1B and S1C). We found that the short (S-), medium (M-), and long (L-) spacer B7-H3 CARs induced lysis and cytokine production *in vitro* against established B7-H3–positive CNS cancer models U87, D283, and PBT-29 (18–20), but not against B7-H3–negative K562 cells (Supplementary Fig. S2A–S2C). Of note, M-spacer B7-H3 CARs elicited the greatest specific lysis against the treatment-naïve biopsy-derived DIPG model PBT-29 (Supplementary Fig. S2B).

We generated glioblastoma xenografts using U87 eGFP:ffluc cells stereotactically implanted into the mouse cerebral hemisphere. Seven days later, mice were treated with a single intracranial dose of untransduced control (mock) versus S-, M-, or L-spacer B7-H3 CAR-expressing CD8+ T cells. Kaplan–Meier analysis of survival (Supplementary Fig. S3A) and serial bioluminescence tumor imaging (Supplementary Fig. S3B and S3C) were performed. S- and M-spacer length B7-H3 CAR T cell–treated mice survived to the planned 90-day study completion, which was a median of 61 days longer than the untransduced mock group (*P* = 0.0004). Based on these results (and the benefit of selecting the smallest functional spacer size to allow for additional cargo), the M-spacer B7-H3 CAR was advanced to a clinical trial.

BrainChild-03: Clinical Trial Design and Initial Cohort of Patients with DIPG

Based on our preclinical findings, Seattle Children's success in delivering CAR T cells with potent antitumor activity (4), and preliminary evidence that repeated locoregional delivery of CAR T cells to patients with CNS tumors was feasible and well tolerated (10), we opened a phase I single-institution clinical trial, BrainChild-03, to accrual in November 2019. This trial delivers repeated locoregional doses of B7-H3 CARs to children and young adults (ages 1–26 years) with recurrent or refractory CNS tumors, including nonpontine diffuse midline glioma [arms A (localized) and B (metastatic)], and DIPG

(arm C) enrolled any time following standard radiotherapy, including children with progression and/or metastatic disease (NCT04185038; Fig. 1A–C). Locoregional delivery [into tumor cavity (arm A) or intraventricular (arms B and C)] was chosen based on our preclinical experience suggesting enhanced efficacy with locoregional dosing and our clinical experience with BrainChild-01 (targeting HER2; ref. 10) and BrainChild-02 (targeting EGFR). Patients with DIPG enrolled on BrainChild-03 arm C receive CAR T cells through a CNS catheter, most often an Ommaya, directed into a lateral ventricle. Lymphodepletion was not incorporated as it is not feasible during a repeated dosing regimen and because there have been objective radiographic responses without lymphodepletion in adult CNS CAR T-cell trials (21, 22). Patients enrolled in arm C received every other week dosing of B7-H3 CARs.

DIPG was defined as either unbiopsied radiographically classic DIPG or, if a biopsy was performed, histopathologic diagnosis of HGG (World Health Organization grade III or IV). Presence of the H3K27M mutation was not required as this arm is dedicated to the pontine location, not a molecular subgroup. Biopsy and/or confirmation of B7-H3 expression was not required for enrollment in the trial due to the known high frequency of B7-H3 expression in these tumors (7, 9, 15). Patients were able to enroll after standard radiation (before or after progression), but most patients with DIPG enrolled on dose regimen 1 (DR1; i.e., DL1) completed multiple tumor-directed therapies prior to CAR T-cell therapy.

Manufacturing and Phenotype of Patient-Derived B7-H3 CAR T-cell Products

CAR T-cell manufacturing used a 1:1 mixture of CD4-enriched and CD8-enriched cell fractions that were pooled at the beginning of cell culture and expanded in the presence of IL7, IL15, and IL21 as previously described (10). However, BrainChild-03 CAR T-cell production incorporated a methotrexate (MTX) selection step, afforded by the introduction of a human DHFR variant, providing resistance to antifolates and allowing for a dominant selectable marker (refs. 23, 24; Supplementary Fig. S4). The MTX-resistant human DHFR mutein (huDHFR^{FS}; L22F, F31S) was incorporated in a single transcript in combination with the B7-H3–specific CAR and truncated EGFR (EGFRt), each separated by a T2A ribosome skip sequence. Expression of huDHFR^{FS} renders polyclonally activated, lentiviral vector (LV) transduced primary human CD4+ and CD8+ T cells resistant to cytocidal concentrations of MTX (25). By combining the human-encoded DHFR mutein with pharmaceutical grade MTX, a purified population of LV transduced B7-H3–specific CAR-expressing T cells can be produced for the clinic in the setting of current good manufacturing practice (GMP)–compliant manufacturing.

All five DIPG patients enrolled in arm C met feasibility for generating a specified CAR T-cell product, with 3.85×10^9 CAR (EGFRt+) T cells generated for S005, 7.84×10^8 for S006, 4.54×10^9 for S007, 4.29×10^9 for S008, and 2.3×10^9 for S014 (Fig. 1D). With an initial seed CD4+:CD8+ ratio of 1:1, the final product CD4+:CD8+ ratios were 34.1:63.5 (S005), 56.1:44.7 (S006), 29:67.9 (S007), 16.5:83.2 (S008), and 38.3:61.3 (S014). The relationship between the input CD4+:CD8+ ratio and that of the final product is best preserved over short culture durations, and the culture durations for S005, S006, S007,
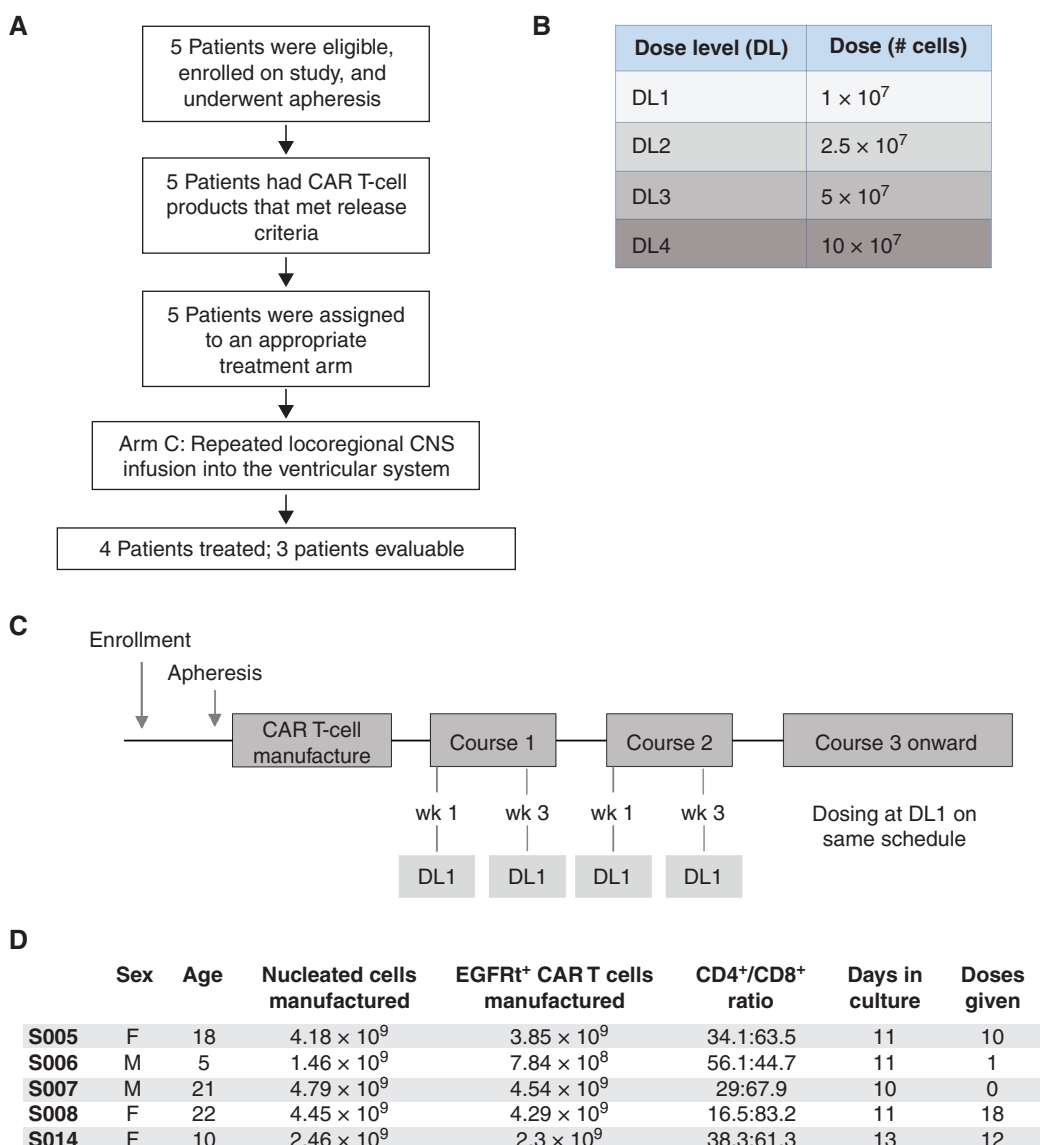
A

5 Patients were eligible, enrolled on study, and underwent apheresis

↓

5 Patients had CAR T-cell products that met release criteria

↓

5 Patients were assigned to an appropriate treatment arm

↓

Arm C: Repeated locoregional CNS infusion into the ventricular system

↓

4 Patients treated; 3 patients evaluable

B

Dose level (DL)	Dose (# cells)
DL1	1×10^7
DL2	2.5×10^7
DL3	5×10^7
DL4	10×10^7

C

Enrollment — Apheresis

CAR T-cell manufacture → Course 1 → Course 2 → Course 3 onward

Course 1: wk 1 (DL1), wk 3 (DL1)
Course 2: wk 1 (DL1), wk 3 (DL1)
Course 3 onward: Dosing at DL1 on same schedule

D

	Sex	Age	Nucleated cells manufactured	EGFRt+ CAR T cells manufactured	CD4+/CD8+ ratio	Days in culture	Doses given
S005	F	18	4.18×10^9	3.85×10^9	34.1:63.5	11	10
S006	M	5	1.46×10^9	7.84×10^8	56.1:44.7	11	1
S007	M	21	4.79×10^9	4.54×10^9	29:67.9	10	0
S008	F	22	4.45×10^9	4.29×10^9	16.5:83.2	11	18
S014	F	10	2.46×10^9	2.3×10^9	38.3:61.3	13	12

Figure 1. BrainChild-03 arm C trial design. **A,** CONSORT diagram of BrainChild-03 arm C interim analysis. Five patients were eligible and underwent apheresis, which led to a CAR T-cell product meeting release criteria in all patients. Four patients advanced to receive CAR T-cell therapy and three patients were evaluable. **B,** Dose levels. **C,** Clinical trial schedule for patients enrolled on dose regimen (DR) 1. By completion of course 2 (the end of the DLT observation window) patients have received 4 doses at DL 1. If study criteria are met, patients may elect to continue beyond course 2 at DL1. **D,** DIPG patient demographics and product characterization.

S008, and S014 were 11, 11, 10, 11, and 13 days, respectively. These data support the ability to generate a mixed CD4+:CD8+ B7-H3 CAR product in an expected time frame.

We analyzed each patient's CAR T-cell infusion product via mass cytometry [i.e., cytometry by time of flight (CyTOF)] using a phenotype panel to assess cell-surface marker expression upon thaw, and a functional panel to further interrogate intracellular cytokine production post stimulation. CD8+ products were phenotypically similar between patients (Supplementary Fig. S5A–S5D) with expression of the activation markers CD38 and CD39 being the only major distinguishing features between clusters. We observed high expression of CD45RA, CXCR3, Ki-67, and CD127, markers associated with proliferative potential and engraftment fitness. The CD8+ product of

S006 was distinct from the others due to an increased proportion of cells identified as CD38hiCD127lo (gray cluster).

After stimulation with PMA/ionomycin (26), we observed six major functional clusters in CD8+ products driven by differences in IFNγ, GM-CSF, and IL2 production (Fig. 2A–C). The majority of cells in each patient's product expressed high levels of IFNγ, GM-CSF, granzyme B, Perforin, and TNFα, but low-to-no PD-1, consistent with activation (Fig. 2A–C, purple cluster; Fig. 2D). The CD8+ product of S006 noticeably lacked the IFNγhiGM-CSFhiIL2hi cluster of cells (magenta) and instead had a higher proportion of IFNγlo cells (green and blue clusters).

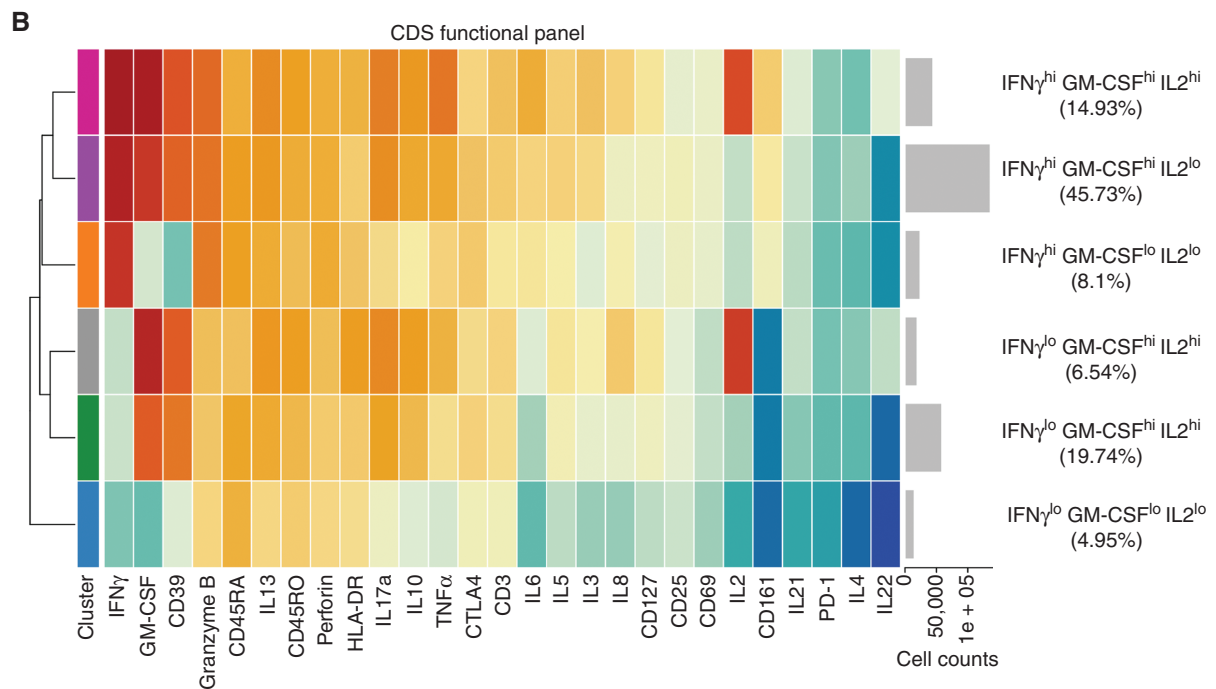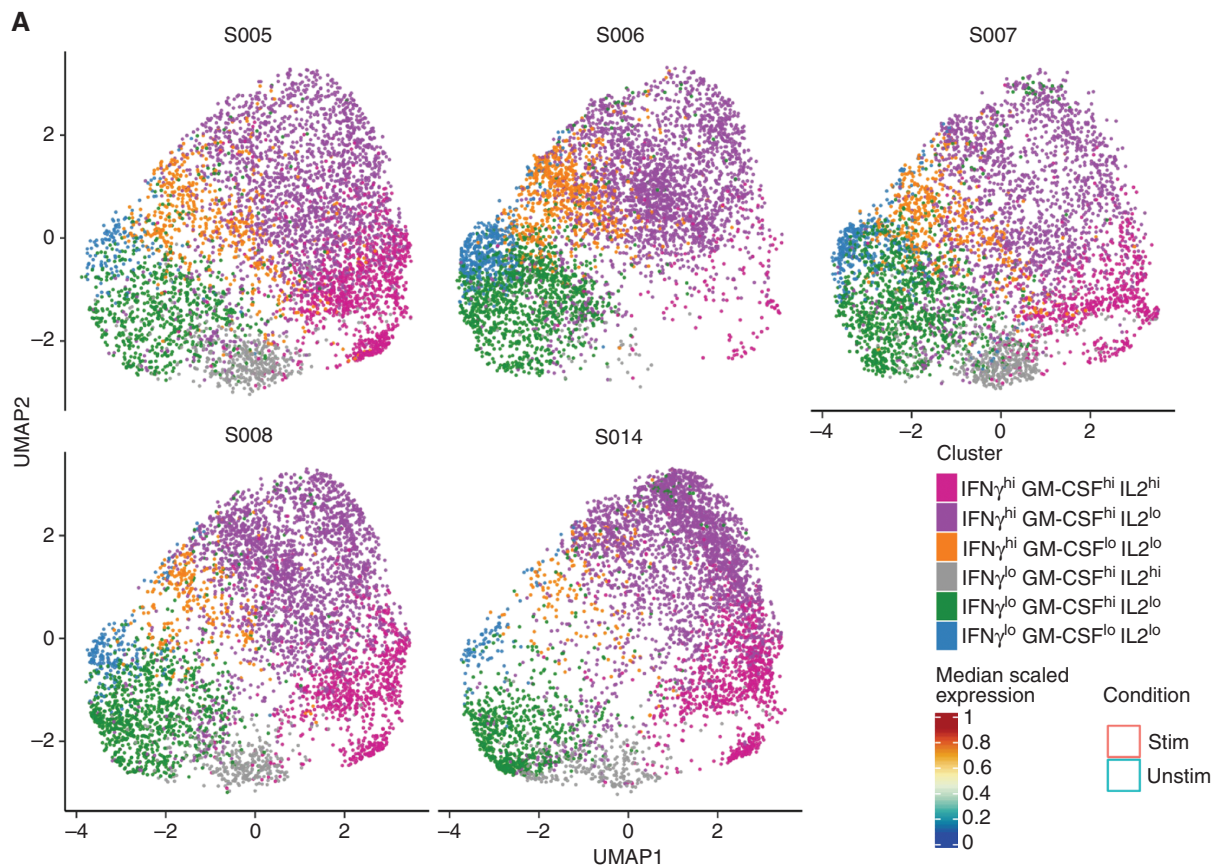CD4+ infusion products were phenotypically and functionally similar post manufacturing (Supplementary Figs.

Figure 2. Functional analysis of stimulated CD8^{+} infusion products by CyTOF. **A,** Uniform manifold approximation and projection (UMAP) representations of the cells. 5,000 cells from each product were used in the UMAP analysis. Cells in the UMAPs were colored by a cluster color designation. **B,** Heat map of cell clusters that constitute stimulated (by PMA/ionomycin) infusion products of all five patients with DIPG. Cell intensity expressions were first normalized from 0 to 1 for each marker. The heat map was then colored using the median of the scaled intensity expressions (between 0 and 1) of each marker. Each row of the heat map was annotated by the cluster color designation, descriptive cluster name, histogram of cell count, and percentage of cell counts. (*continued on following page*)

C

D
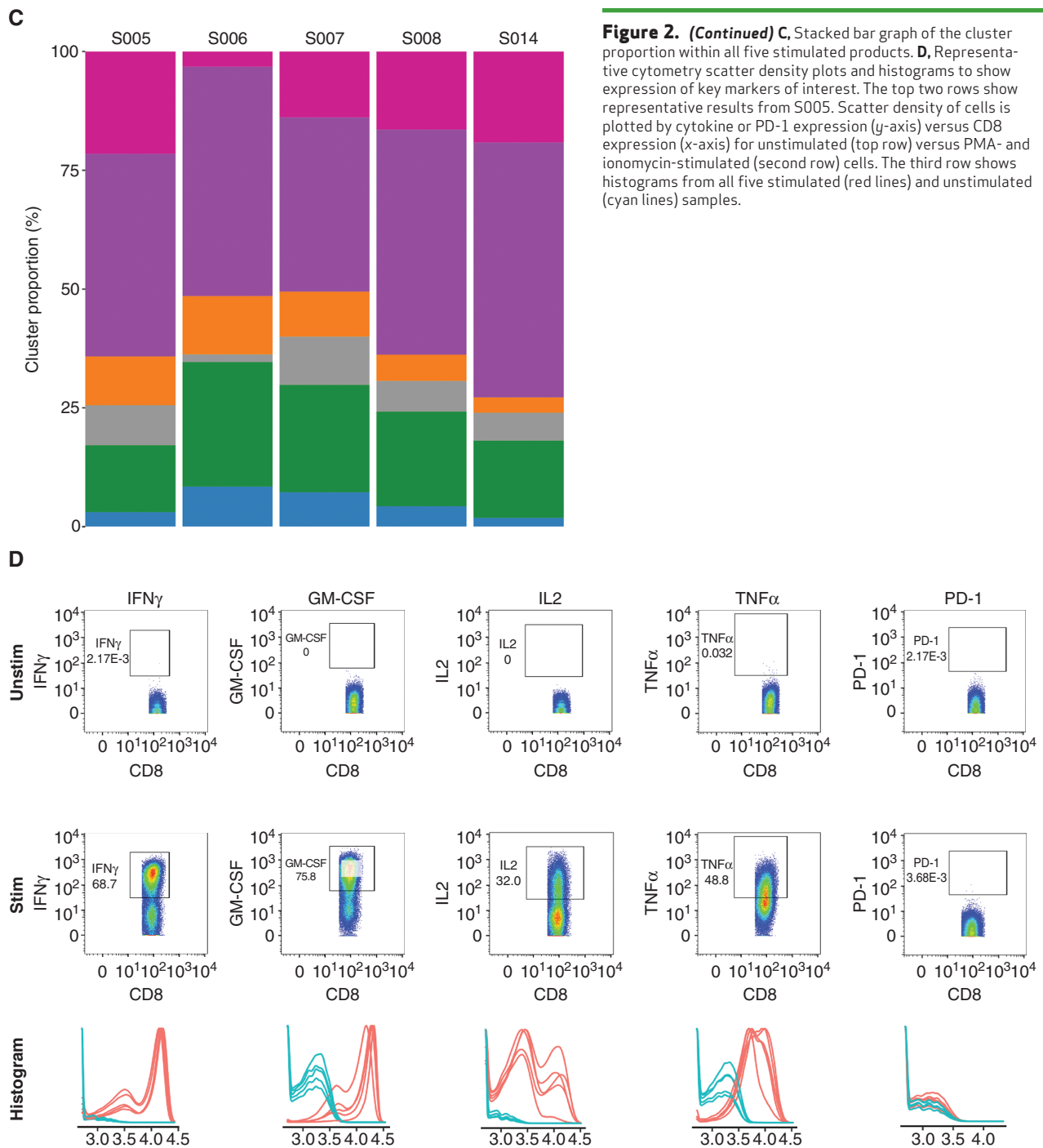
Figure 2. *(Continued)* **C,** Stacked bar graph of the cluster proportion within all five stimulated products. **D,** Representative cytometry scatter density plots and histograms to show expression of key markers of interest. The top two rows show representative results from S005. Scatter density of cells is plotted by cytokine or PD-1 expression (*y*-axis) versus CD8 expression (*x*-axis) for unstimulated (top row) versus PMA- and ionomycin-stimulated (second row) cells. The third row shows histograms from all five stimulated (red lines) and unstimulated (cyan lines) samples.

S6A–S6D and S7A–S7D). We observed three phenotypic clusters driven by differential expression of CXCR3 and CCR4 (Supplementary Fig. S6A–S6C). CD4$^+$ products were predominantly CXCR3^{hi}CCR4^{hi} and Ki-67^{hi} (magenta cluster), with the exception of S006's product, which had a higher proportion of CAR T cells that were CCR4^{lo}. Upon stimulation, CD4$^+$ products produced high levels of IL2, GM-CSF, and CD39 (Supplementary Fig. S7), whereas the CD4$^+$ product of S006 had a noticeable increase in cells that were IL2^{lo}.

Assessment of the memory profile in the CD4$^+$ and CD8$^+$ infusion products showed that cells were predominantly CCR7$^−$CD45RA$^−$, suggesting an effector memory–like status (Supplementary Fig. S8A and S8B). A majority of cells were also CD69$^−$CD39$^−$, a recently described stem-like phenotype associated with improved expansion and persistence (Supplementary Fig. S8C and S8D; ref. 27). CD8$^+$ infusion products also had a large proportion of CD69$^−$CD39$^+$ cells indicating an activated state without terminal differentiation. CD69$^+$CD39$^+$ double-positive cells, which have been associated with poor persistence (27), constituted a negligible portion of B7-H3 CAR products. Only S006's CD8$^+$ infusion product had a measurable CD69$^+$CD39$^+$ population (6.48%

of the CD8$^+$ population; Supplementary Fig. S8D). Together, these data suggest the utility of our updated manufacturing strategy including the use of MTX selection to produce activated, proliferating, polyfunctional, cytokine-producing CAR T cells that express phenotypic markers of engraftment fitness.

Repetitive Intraventricular B7-H3–Specific CAR T-cell Infusions Were Well Tolerated in the First Three Evaluable Patients with DIPG

Patients enrolled on arm C are defined as evaluable for the primary endpoint of establishing safety after completion of two courses (i.e., four infusions of B7-H3 CARs) or earlier if dosing is suspended due to the occurrence of a dose-limiting toxicity. The initial three evaluable patients with DIPG received weekly fixed doses of 1×10^7 B7-H3 CARs, with a total of 40 B7-H3 CAR infusions, including 10 infusions, 18 infusions, and 12 infusions for S005, S008, and S014, respectively. S006 and S007 were not evaluable. S006 had received multiple prior therapies and experienced multiple disease progressions. Following a single CAR T-cell infusion, the patient continued to progress clinically, so it was determined by the principal investigator and the patient's family that it was in the patient's best interest to redirect to supportive care. S007 experienced rapid disease progression following apheresis and was never able to receive a CAR T-cell dose.

The most consistent adverse events possibly, probably, or definitely related to CAR T-cell infusions were headache (3/3), nausea/vomiting (3/3), and fever (3/3) usually beginning within 24 hours of infusion and returning to baseline within 72 hours (Supplementary Fig. S9; Supplementary Table S1). In each instance, the patient returned to baseline without the use of steroids or cytokine antagonists. S005 experienced worsened pontine-related symptoms including gait disturbance and dysphagia following her eighth dose but returned to baseline within 48 hours. No patient experienced a dose-limiting toxicity (DLT), while on protocol therapy, no patients received anakinra, bevacizumab, dexamethasone, or tocilizumab and no patients required pediatric intensive care unit admission.

Clinical and Neuroimaging Outcomes of the First Three Evaluable Patients with DIPG Receiving B7-H3 CAR T Cells

Patients had neuroimaging performed following every 2 courses (i.e., 8 weeks) as per the protocol's scheduled observations (Fig. 3A–I). Following ~6 months on protocol therapy both S005 (pontine DMG, H3K27M-altered) and S014 (unbiopsied, H3K27M mutation detected in plasma), who both enrolled after initial tumor progression, demonstrated increased tumor bulk with infiltration in the right brachium pontis and dentate nuclei (Fig. 3A–C and G–I). S008 (pontine anaplastic astrocytoma; histone 3 wild-type; *TP53* and *IDH1* mutant), who enrolled prior to progression, demonstrated a mild decrease in tumor size (19.4% decrease from the baseline sum of the longest perpendicular diameters) and less conspicuity of T2 hyperintense tumoral nodules on imaging 307 days from her initial infusion (Fig. 3D–F). By the timing of the eighth CAR T-cell dose, S008's baseline grade 1 facial nerve palsy improved, with sustained improvement through 12 months on study, at which time she elected to

discontinue protocol therapy and change to a treatment at her home institution.

No patients demonstrated radiographic evidence of elevated intracranial pressure (ICP), clinical signs of herniation, or required acute neurosurgical interventions. S005 with progressive disease remains alive 17 months from enrollment and 36 months from diagnosis; S008 with stable disease remains alive 16 months from enrollment and 20 months from diagnosis. S014 with progressive disease remains alive 12 months from enrollment and 26 months from diagnosis. S005 and S014, the two evaluable patients who enrolled after progression, have survived 494 and 328 days after initial CAR T-cell infusion (Supplementary Fig. S10).

B7-H3 CAR T Cells Were Detectable in the CSF of DIPG Patients Post Infusion

We performed flow cytometry on serial CSF biospecimens to identify CAR T cells. We detected circulating EGFRt$^+$ CAR T cells in the CSF of two of three evaluable patients (S005 and S008; Fig. 4A–C; Supplementary Figs. S11 and S12; Supplementary Table S2). CSF biospecimens were infrequently available for S014 due to neurosurgical guidance not to draw back from her Ommaya (based on its location, though infusion was uncomplicated) and, in the few samples available, CAR T cells were not detected. S005 had detectable CAR T cells at course 3 week 4 (5 days after prior infusion) just above the limit of detection (0.84% EGFRt$^+$ of lymphocytes; Supplementary Fig. S11A and S11B), whereas S008 had detectable CAR T cells at several time points throughout protocol therapy. Peak detection in S008 was observed at course 1 week 3 after infusion, where 64% of detectable lymphocytes in the CSF were B7-H3 CARs (EGFRt$^+$) and B7-H3 CARs were predominantly CD8$^+$ (Fig. 4B and C; 85% CD8$^+$EGFRt$^+$ and 15% CD4$^+$EGFRt$^+$). CAR T cells persisted in S008 through course 9, after which only preinfusion biospecimens were collected and we did not detect CAR T cells. We also observed increased non-CAR (EGFRt$^-$) CD3$^+$ cells in the CSF after initial infusion in both S005 and S008, similar to our previous report post infusion of HER2 CAR T cells (10). We did not detect CAR T-cell DNA (via qPCR) in the peripheral blood of any patient at any time point tested (Supplementary Table S3).

Cytokine Analysis and Targeted Mass Spectrometry in the CSF and Serum of Patients with DIPG Receiving B7-H3 CAR T Cells

We next measured chemokine/cytokine levels in CSF (Fig. 5) and serum (Supplementary Fig. S13) from patients at various time points throughout their CAR T-cell infusion schedule. After the initial infusion, patients had detectable levels of the following analytes in the CSF: CCL2, CXCL10, G-CSF, GM-CSF, IFNα2, IFNγ, IL10, IL12p40, IL12p70, IL15, IL1α, IL3, IL6, IL7, TNFα, and VEGF. Compared with preinfusion, patients demonstrated elevations in multiple chemokines and cytokines, including CCL2, CXCL10, GM-CSF, IFNγ, IL15, IL1α, IL6, and TNFα (Fig. 5). Similar to our previous report of patients receiving intracranial HER2 CAR T cells (10), CCL2 (S005: maximum concentration of 3,144.13 pg/mL; S008: maximum concentration of 14,284.44 pg/mL) and CXCL10 (S005: maximum concentration of 3,063.41 pg/mL; S008: maximum concentration of 4,160.84 pg/mL)
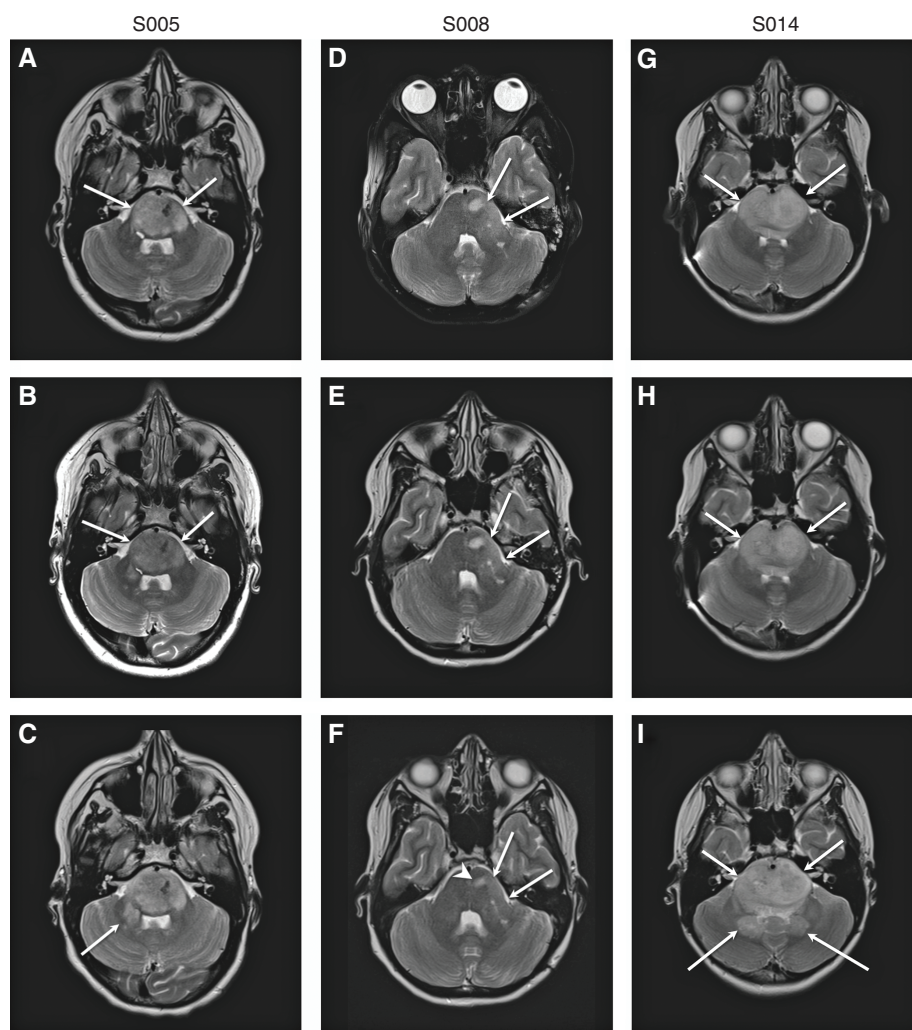
Figure 3. Neuroimaging after locoregional B7-H3 CAR T-cell infusion. MRI images from S005 (**A–C**), S008 (**D–F**), and S014 (**G–I**). Axial T2-weighted images from all three patients immediately before initial CAR T-cell administration (**A, D**, and **G**), following course 2 (i.e., 4 intracranial B7-H3 CAR T-cell infusions; **B, E**, and **H**), and prior to any other tumor-directed therapy (**C, F**, and **I**). Images correspond to study participants S005 (**A–C**; imaged at days −2, 53, and 138 relative to first infusion), S008 (**D–F**; imaged at days −19, 50, and 307 relative to first infusion), and S014 (**G–I**; imaged at days −1, 45, and 211 relative to first infusion). Patients S005 and S014 experienced slow progression in tumor bulk over time, with increased tumor infiltration in the right brachium pontis (arrow in **C**) and dentate nuclei (posterior arrows in **I**). Patient S008 showed mildly decreased tumor bulk (long arrows in **F**) and decreased conspicuity of T2 hyperintense tumoral nodule (short arrowhead in **F**).

were the most elevated chemokines detected, whereas serum cytokine levels appeared relatively stable in both patients across all CAR T-cell infusions, with fewer fluctuations compared with CSF.

Finally, we performed multiple reaction monitoring-mass spectrometry (MRM-MS) on serial CSF and serum biospecimens to establish the feasibility of this analytic approach and to explore the utility of targeted proteomics in the setting of immune and tumor responses. MRM-MS is a targeted form of mass spectrometry that has been well demonstrated for the quantification of peptides and proteins (28). By combining peptide immunoaffinity enrichment with MRM-MS, immuno-MRM assays can be applied for sensitive measurement of proteins in human cancer tissues and fluids (29–47). We have evaluated this approach for the measurement of immunomodulatory proteins using longitudinal biospecimens from two BrainChild-03 DIPG patients, where we detected 50 (CSF) and 59 (serum) proteins above the lower limit of quantification.

In general, there were fewer protein fluctuations in the serum compared with the CSF, supporting that inflammatory activity is increased locally in the CNS compared with the systemic circulation following intracranial CAR T-cell infusions (Fig. 6A and B; Supplementary Fig. S14A and S14B). For

example, sharp increases of several immunoregulatory peptides were measured locally in the CSF at postinfusion time points as compared with their preinfusion values, including BCL10, CXCL13, HAVCR2 (TIM-3), ICOSLG (ICOS ligand), PDCD1LG2 (PD-L2), TNFRSF14 (TNF receptor superfamily member 14), and VCAM-1, compared with more gradual trends in serum (Fig. 6; Supplementary Fig. S14). Notably, several analytes tracked consistently in the CSF of both patients, including markers of macrophage maturation and proteins involved in immune cell recruitment, including CD14, CD163, CD44, CSF-1, CXCL13, and VCAM-1 (Fig. 6A and B). Changes in a minority of analytes were patient-specific, for example, in overall expression levels [e.g., ALCAM, IDO1, MSH6, and TNFRSF17 (BCMA)], in the shape of profiles measured over the course of treatment (e.g., BTK and CD47), or in features with a sharp elevation late in the course of therapy (e.g., ANXA1, PSMA1, STAT6, TAPBP, and XRCC5).

CD276 (B7-H3) protein was detected in the CSF and serum of both patients. S005, who progressed on protocol therapy, had a sharp increase in the CSF during course 2, whereas S008, who had clinical improvement on protocol therapy, had consistently lower CD276 present (Fig. 6A). Notably, serum B7-H3 steadily declined in both patients over time, with the
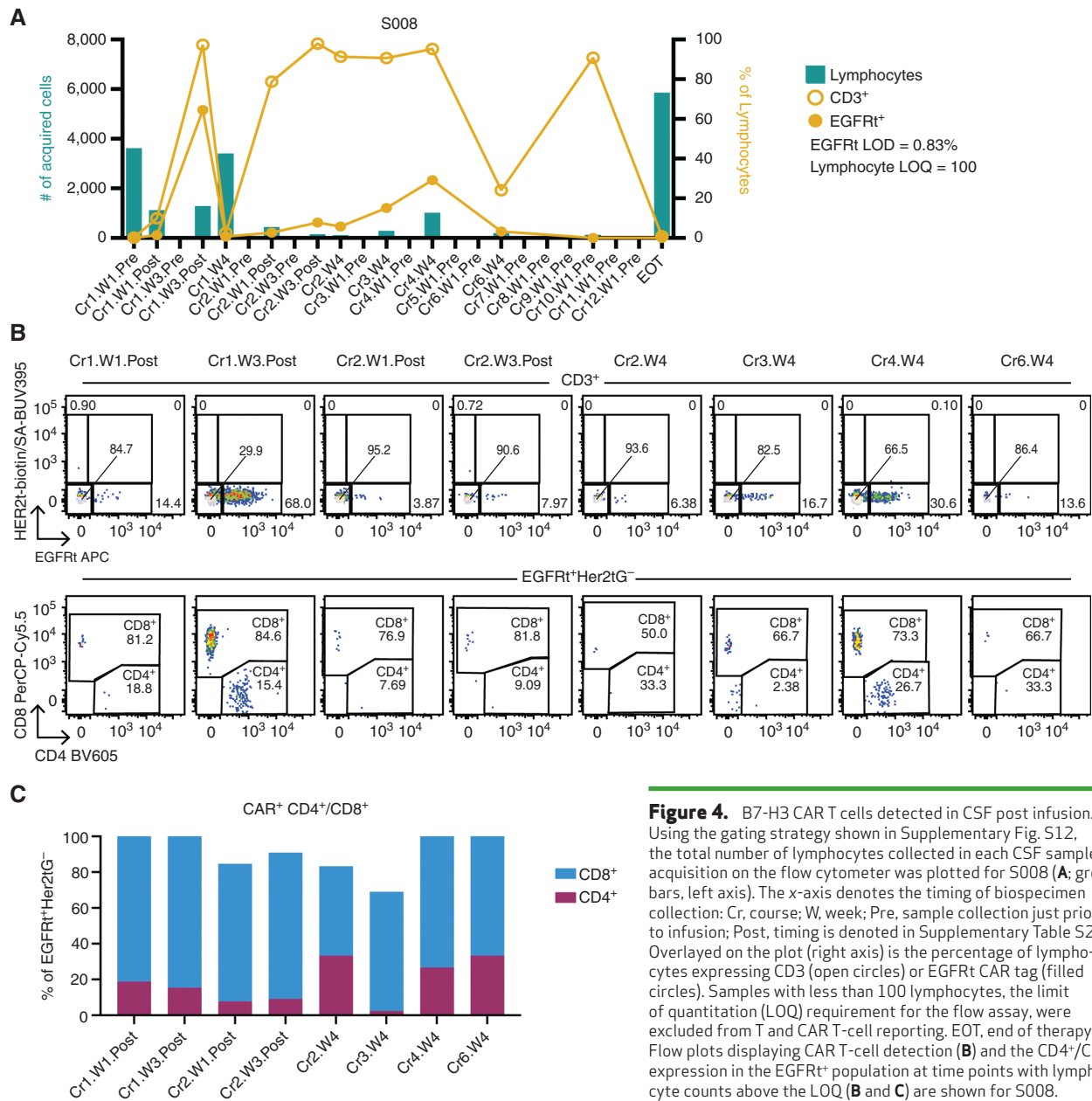
Figure 4. B7-H3 CAR T cells detected in CSF post infusion. Using the gating strategy shown in Supplementary Fig. S12, the total number of lymphocytes collected in each CSF sample acquisition on the flow cytometer was plotted for S008 (**A**; green bars, left axis). The x-axis denotes the timing of biospecimen collection: Cr, course; W, week; Pre, sample collection just prior to infusion; Post, timing is denoted in Supplementary Table S2. Overlayed on the plot (right axis) is the percentage of lymphocytes expressing CD3 (open circles) or EGFRt CAR tag (filled circles). Samples with less than 100 lymphocytes, the limit of quantitation (LOQ) requirement for the flow assay, were excluded from T and CAR T-cell reporting. EOT, end of therapy. Flow plots displaying CAR T-cell detection (**B**) and the CD4^{+}/CD8^{+} expression in the EGFRt^{+} population at time points with lymphocyte counts above the LOQ (**B** and **C**) are shown for S008.

exception of a transient increase in S005 between courses 4 and 5 (Supplementary Fig. S14). Also, C-reactive protein and CXCL10 were detected in the CSF of S008, but not S005.

Along with chemokine/cytokine analysis, targeted serial proteomic assessments supported local CNS immune activation and detected declining serum levels of B7-H3 throughout protocol therapy with B7-H3 CARs. Future work will explore the correlation of these measurements with clinical endpoints for potential use as markers of efficacy of therapy or adverse events.

DISCUSSION

We present the preclinical development of a B7-H3 CAR T-cell product intended for therapeutic treatment of pediatric CNS tumors and the preliminary clinical and correlative experience from BrainChild-03, Seattle Children's phase

I clinical trial delivering locoregional B7-H3 CARs of a mixed CD4^{+}:CD8^{+} ratio for children and young adults with recurrent/refractory CNS tumors and DIPG. Although other groups have preclinically studied genetically modified cellular products targeting B7-H3 (9, 11–16), here, we demonstrate the feasibility and preliminary tolerability of repetitive intraventricular doses as a strategy to fractionate dosing for improved tolerability, and, as a strategy to replenish bioactive B7-H3 CAR T cells in children and young adults with CNS tumors. In addition, we show correlative cytokine data consistent with proinflammatory immune cell activity in the CSF and demonstrate that the B7-H3 CAR T cells can persist in the CSF following locoregional delivery. We also demonstrate the feasibility of targeted, immuno-MRM performed on serum and CSF biospecimens.

In our initial cohort of DIPG patients enrolled on DR1, we were able to manufacture sufficient B7-H3 CARs (mean of
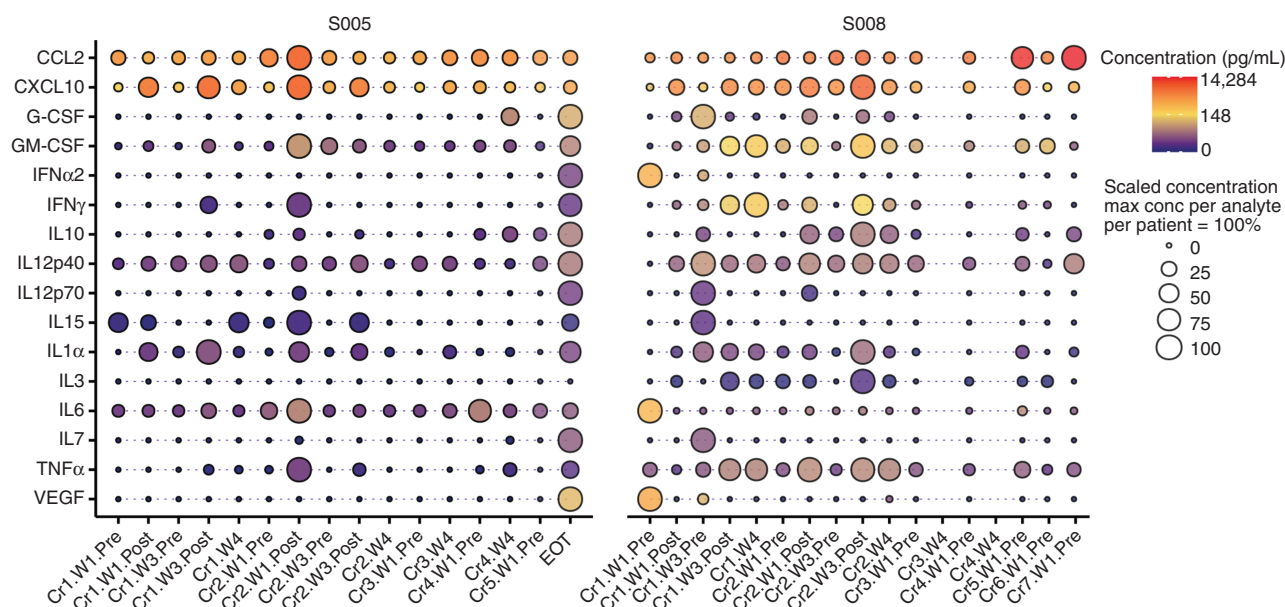
Figure 5. High concentrations of CXCL10, CCL2, and GM-CSF are detected in CSF after treatment. Cytokine concentrations in CSF across both patients were converted to log2 scale and represented with circles filled with color. Red color corresponds to the highest log2 concentration measured across both patients. Yellow and blue colors correspond to 50% and 0% of the log2 concentration, respectively. Additionally, concentrations relative to the maximum concentration observed for a given patient and analyte are represented by the size of the circles, to highlight the fluctuation in cytokine concentrations throughout a patient's CAR T-cell treatment. The x-axis denotes the timing of biospecimen collection: Cr, course; W, week; Pre, sample collection just prior to infusion; Post, timing is denoted in Supplementary Table S2. EOT, end of therapy.

4.56×10^9 cells per patient) for repeated dosing in a protocol-driven time frame in all five patients. Final products across all five patients expressed high levels of CD127, CD45RA, CXCR3, CCR4, and Ki-67, and low levels of PD-1, supporting that our CAR T cells maintain proliferative potential and engraftment fitness as desired for an infused cellular product (48). B7-H3 CAR products were also predominantly CD69⁻CD39⁻, a phenotype associated with expansion and persistence (27). Notably, ligands for CXCR3 and CCR4 are CXCL10 and CCL2, respectively, the chemokines detected at the highest levels in the CSF post B7-H3 CAR T-cell infusion. Clinically, S006 continued a consistent trajectory of rapid progression following one B7-H3 CAR T-cell dose, which may underscore the need for repeated dosing or may simply indicate the treatment was initiated at too late a clinical time point to offer any benefit. The CAR T-cell product for S006 also had some unique features. The CD38hi CD127lo IFNγlo CD8+ and the CD45RAhi CD38hi CD39hi CD127lo IL2lo CD4+ CAR T cells could represent a greater degree of differentiation that may be associated with poorer fitness or limited proliferative capacity. S006's CD8+ product also had a small, but detectable, CD69+CD39+ population, which has been associated with poor persistence (27). However, this is within the context of the patient's clinical rapid progression that by historical experience was most likely unable to be reversed. Immune effector cell characteristics and function are known to vary by age (49, 50) and the median age of the initial 3 enrolled patients is above the historical median age for children with DIPG. As the median age of enrolled children likely moves to historical averages (~6 years of age; ref. 1), we will assess if B7-H3 CAR T-cell product function and immunologic responses correlate with patient age. Additionally, we have previously described the MTX selection process (24), but for individual patient products, we did not

explore a comparison with our prior manufacturing strategy without MTX selection, which limits the ability to claim superiority of either manufacturing approach.

The extended survival of S005 and S014 post initial CAR T-cell infusion is promising, especially given preenrollment clinical and radiographic progressive tumors that did not receive reirradiation before starting protocol therapy, although survival conclusions cannot be drawn from such a preliminary experience. A recent case report of intracavitary B7-H3 CAR T cells for a 56-year-old with glioblastoma did show a transient radiographic response as well as tolerability with repeated infusions (22) and another case report of a 49-year-old with anaplastic meningioma also showed tolerability of intracavitary infusions (51). In both cases, patients experienced headaches following infusion similar to our experience.

B7-H3–specific CAR T cells were detected post infusion in the CSF from both patients for whom serial CSF biospecimens were evaluable, in contrast to our HER2 CAR T-cell experience in which CSF CAR T cells were undetectable. The increased CAR T-cell presence may be related to the B7-H3 CAR itself, the anatomic location of DIPG, or the nonimmunosuppressive environment of these tumors (8). S008, who received 18 doses over approximately 1 year on protocol therapy, had circulating CSF CAR T cells detected at multiple time points that may be related to her clinical improvement and lack of progression while on protocol therapy, although an *IDH1*-mutant HGG is biologically less aggressive than those harboring mutations in H3K27M. As more patients with DIPG become evaluable, we will determine if the magnitude and duration of B7-H3 CAR T-cell persistence corresponds to response by clinical and neuroimaging criteria. BrainChild-03 does not require IHC of tumor B7-H3
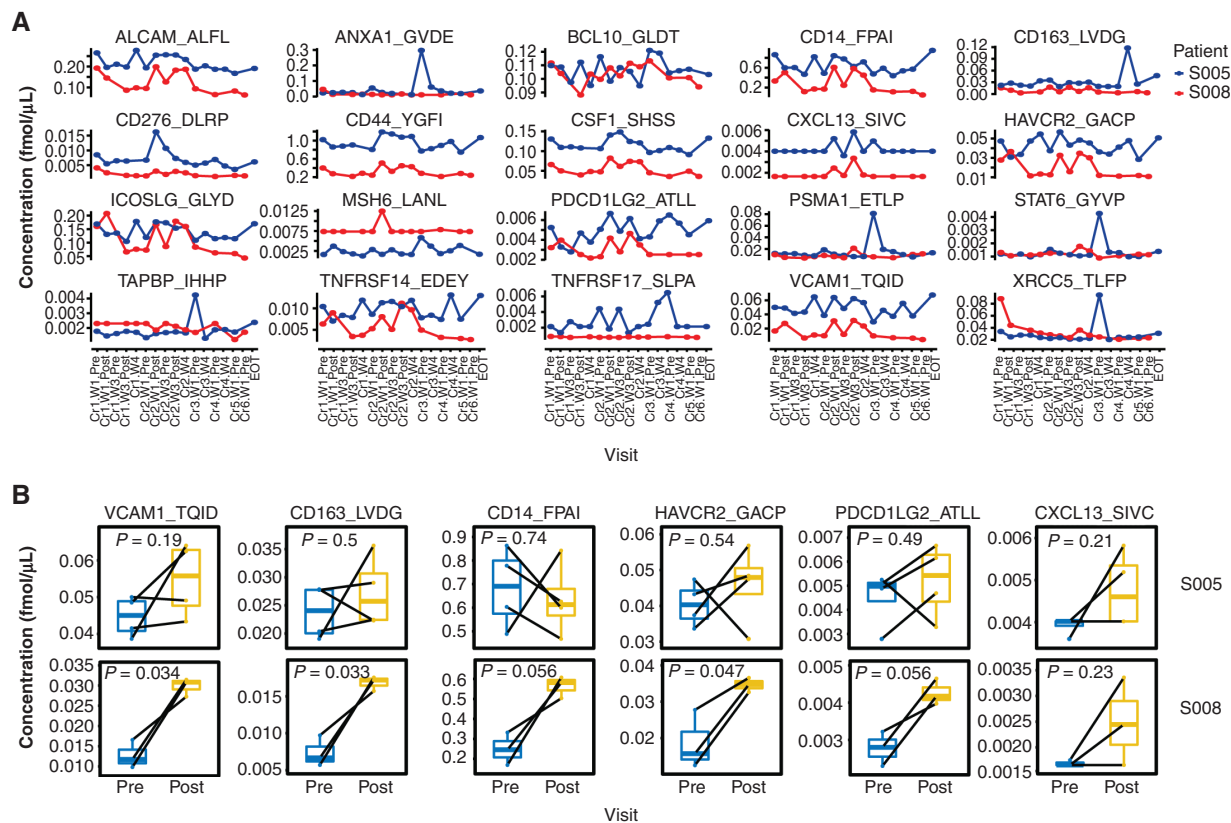
Figure 6. Targeted proteomics supports local immune activation during intracranial B7-H3 CAR T-cell therapy. **A,** Targeted immuno-MRM peptide concentrations in CSF plotted versus visit for patients S005 (blue) and S008 (red). Analyte name is represented by a gene symbol followed by the first four amino acids of the target peptide. Only peptides detected above the lower limit of quantification in at least one visit from both patients were plotted. The x-axis denotes the timing of biospecimen collection: Cr, course; W, week; Pre, sample collection just prior to infusion; Post, timing is denoted in Supplementary Table S2. EOT, end of therapy. **B,** Concentrations for selected peptides in all pairwise pre- and posttreatment samples. Box plots represent median (bar), lower and upper quartiles (box), and 5th–95th percentiles (vertical line). Pairs of pre- and posttreatment samples are connected by a black line.

expression due to the high expression of B7-H3 on pediatric CNS tumors (7, 9, 15) and because an antibody for B7-H3 was not available in a CLIA-certified environment at the initiation of this trial. Therefore, although unlikely, there may be enrolled patients whose tumor does not express B7-H3 and CAR T-cell persistence could be related to tumor B7-H3 expression. We will attempt to assess this in future cohorts.

Similar to our experience in the BrainChild-01 trial using intracranial HER2 CARs (10), CCL2 and CXCL10 were the most elevated chemokines detected in the CSF and frequently demonstrated increases post CAR T-cell infusion, while serum chemokines and cytokines remained relatively stable. Serial liquid disease monitoring of relevant immunomodulatory proteins and tumor antigens via targeted, immune-MRM mass spectrometry was feasible in our initial attempt in both patients for whom biospecimens were available as 50 and 59 proteins were detectable in CSF and serum, respectively. We will continue this analysis in a larger cohort of treated patients, which may help to interrogate local immune activation and provide deeper insight into supportive or antagonist immune cell populations. Of note, the mass spectrometry immuno-oncology panel did not include H3K27M but it will be incorporated into future analysis once it is validated. As CD276 (B7-H3), our CAR T-cell target and

highly expressed on DIPG, rose in S005 who progressed on protocol therapy, targeted MRM analysis may serve as a surrogate marker for tumor/stroma responses to therapy. This may be critical considering the limitations of neuroimaging in the setting of pseudoprogression by immunotherapy.

B7-H3 may offer a therapeutic window providing efficacy and tolerability, though cure may ultimately demand multiantigen CAR T-cell targeting or multimodal therapeutic approaches. We have opened two additional locoregional CAR T-cell clinical trials: BrainChild-01 (NCT03500991; ref. 10) and BrainChild-02 (NCT03638167) delivering HER2-specific (10) or EGFR-specific CAR T cells (19), respectively, to children with recurrent/refractory CNS tumors, so safety data will be available for the single antigen targeting of HER2, EGFR, and B7-H3 through our BrainChild program. As a strategy to overcome tumor target antigen heterogeneity, our next trial will deploy a multiplexed targeting strategy by generating products expressing each of these three CARs, as well as, an IL13zetakine CAR. Additional genetic modifications may also be necessary to improve CAR T-cell persistence (52), the retention of effector function, and trafficking to tumor (53). DIPG tumors may also recruit immunoregulatory microglia and myeloid populations that limit CAR T-cell efficacy (54) as our MRM-MS data revealed heightened

levels of macrophage markers such as CD14, CD163, CSF-1, and PD-L2.

Although there is preclinical work showing the superiority of locoregional B7-H3 CAR T-cell delivery (55, 56) and several cases of tumor regression in the setting of locoregional delivery (5, 21, 22), this has not been validated clinically and locoregional delivery does require infrastructure commitments and repeated dosing. All three of our active trials incorporate locoregional delivery, due to hypothesized improved efficacy by delivering CAR T cells beyond the blood–brain barrier and potentially lower incidence of cytokine release syndrome (CRS) and immune effector cell–associated neurotoxicity syndrome in children who already have significant neurologic dysfunction. Currently, intratumoral CAR T cells are not being used clinically for DIPG, although intratumoral delivery of the oncolytic virus DNX-2401 prior to radiotherapy was shown to be feasible and result in a median survival of 17.8 months (57). We hope the pediatric neuroimmuno-oncology community will work together to define optimal routes of delivery and dosing regimens for these novel therapies.

As patients continue to enroll through a potential dose of 10×10^7 cells, we will continue to assess safety and potential efficacy through a planned expansion cohort of the maximally tolerated dose regimen. In addition, correlative studies such as cytokine analysis and targeted mass spectrometry from serial CSF biospecimens may serve as an early determinant of response or treatment failure, and potentially also be predictive of tumor evolution and optimal next therapy. Ultimately, the experience of the initial three evaluable patients with DIPG treated on BrainChild-03 suggests that the repetitive intraventricular delivery of B7-H3 CAR T cells in high-risk patients may be feasible and result in circulating CNS CAR T cells capable of local immune activation.

METHODS

Design of DNA Constructs and Lentivirus

B7-H3 CAR T cells were developed using scFv binders derived from the MGA 271 (huBRCA84D) monoclonal antibody. The second-generation, 4-1BB costimulated CARs were expressed in lentivirial transfer vector epHIV7.2, a derivative of epHIV7 (24) in which the ampicillin selection marker was exchanged for kanamycin and the CAR-adjacent promoter was replaced with the elongation factor-1 alpha (EF1α core promoter, 230 bp). Variable short (S), IgG4-hinge; medium (M), IgG4-hinge-CH3; long (L), IgG4-hinge-CH2-CH3 second-generation 41BB-CD3ζ CARs were constructed using the V_L and V_H segments of MGA271, similar to those previously described (10, 58, 59). Each CAR sequence was appended to a T2A ribosomal skip sequence followed by a truncated EGFR (EGFRt) cell-surface tag to facilitate selection (60). Lentivirus was produced in HEK 293T cells using the packaging vectors pCHGP-2, pCMV-Rev2, and pCMV-G (58, 61, 62). In addition, the MTX-resistant human DHFR mutein (huDHFR^{FS}; L22F, F31S) was appended after EGFRt by a T2A linker to the BrainChild-03 clinical construct (B7-H3 CAR M-spacer) to allow the use of MTX to select and enrich activated, proliferating CAR T cells *ex vivo*.

Production of Primary T-cell Lines Expressing B7-H3 CARs for Preclinical Analyses

CD4$^+$ and CD8$^+$ bulk T cells were isolated from peripheral blood mononuclear cells of healthy donors (Bloodworks Northwest) by sequential positive selection using CD4 and CD8 microbeads (Miltenyi Biotec). Following isolation, T cells were stimulated with anti-CD3/CD28 Dynabeads (Life Technologies) and transduced at a multiplicity of infection of 3 on the third day of culture. EGFRt-positive T-cell subsets were enriched by immunomagnetic selection using biotinylated cetuximab and antibiotin microbeads (Miltenyi Biotec). Post selection, cells were cryopreserved until further use. Cryopreserved cells were thawed and stimulated with irradiated TM-LCL feeder cells according to rapid expansion protocol. T cells were maintained in RPMI medium (Gibco) supplemented with 10% fetal bovine serum (Seradigm), 2 mmol/L L-glutamine (Gibco), and 0.5 ng/mL recombinant human IL15 (Miltenyi Biotec), CD8$^+$ T cells were maintained with the addition of 50 Seattle Units recombinant human IL2 (Chiron Corporation) and CD4$^+$ T cells were maintained with the addition of 5 ng/mL recombinant human IL7 (Miltenyi Biotec).

Preclinical Flow Cytometry and Immunophenotyping

Tumor cell B7-H3 positivity was confirmed using a PE-conjugated CD276 (B7-H3) antibody (BioLegend). CAR construct expression, via the surrogate cell-surface marker EGFRt, was confirmed using biotinylated cetuximab, and PE-conjugated streptavidin (SA-PE; BioLegend). CAR cell-surface expression was additionally confirmed using biotinylated Protein-L (GenScript) and SA-PE, and total expression was evaluated using anti-CD247 (CD3ζ, BD Biosciences). Flow analysis was performed on an LSRFortessa (BD Biosciences), and data were analyzed using FlowJo software (BD Biosciences).

Cell Line Derivation and Analysis

The U87 and D283 cell lines were obtained from the ATCC. These cell lines were maintained in DMEM (Gibco) supplemented with 2 mmol/L L-glutamine, 25 mmol/L HEPES (Gibco), and 10% heat-inactivated FCS. The previously described biopsy-derived treatment-naïve DIPG cell culture PBT-29 was maintained in the NeuroCult NS-A Basal Medium with NS-A Proliferation Supplement (STEMCELL Technologies), 1× antibiotic/antimycotic (Thermo Fisher Scientific), 40 ng/mL epidermal growth factor (PeproTech), and 40 ng/mL fibroblast growth factor (PeproTech; refs. 18, 20). Relevant cell lines were authenticated by STR profiling matched to the DSMZ Database (University of Arizona Genetics Core). The U87 eGFP:ffluc tumor cells were generated by lentiviral transduction and sorted by FACSAriaII (BD). The K562 B7-H3 knockout (KO) tumor cells were generated from a K562 parental line gifted by S. Riddell (Fred Hutch) and maintained in RPMI (Gibco) supplemented with 2 mmol/L L-glutamine, and 10% heat-inactivated FCS. B7-H3 KO was achieved by transfecting pX459 vector containing a CRISPR target against B7-H3 exon 4 and magnetic-activated cell sorting (Miltenyi Biotec). Following depletion, cells were clonally selected by single-cell limiting dilution.

In Vitro Cellular Assays

Chromium Release Assay. B7-H3 CAR CD8$^+$ T-cell cytotoxicity was determined by the chromium release assay. Target cells were labeled with ^{51}Cr (PerkinElmer), washed, and incubated with T cells at various effector-to-target (E:T) ratios. Supernatants were harvested 4 hours later for γ-counting using a TopCount NXT Microplate scintillation and Luminescence counter (PerkinElmer) and specific lysis was calculated using the standard formula (63).

Cytokine Release Assay. To investigate cytokine secretion, B7-H3 CAR CD8$^+$ T cells and target cells were plated at a 2:1 ratio and the supernatant was analyzed for IL2, IFNγ, and TNFα production after 24-hour incubation using the Bio-Plex multiplex bead array system (Bio-Rad). *In vitro* cytotoxicity and cytokine release assays were performed in triplicate and repeated for validity.

Orthotopic Xenograft Model and Exogenous T-cell Transplantation

All animal experiments were approved by the Seattle Children's Research Institute Animal Care and Use Committee. The orthotopic

xenograft model was performed as previously described (19). Briefly, 8- to 12-week-old adult male NOD-scid IL2Rγnull mice were injected intracranially (i.c.) on day 0 with 2×10^5 eGFP:ffluc expressing U87 tumor cells 2 mm lateral, 0.5 mm anterior to the bregma, and 2.25 mm deep from the dura. On day 7, mice were i.c. injected with a total of 2×10^6 B7-H3 CAR CD8+ T cells 2.5, 2.35, and 2.25 mm deep from the dura. Bioluminescent imaging was performed weekly by intraperitoneal (i.p.) injection of 4.29 mg/mouse D-luciferin (Xenogen) after anesthetization by isoflurane. Imaging occurred 15 minutes after D-luciferin injection using the IVIS Spectrum Imaging System (PerkinElmer). Luciferase activity was analyzed using Living Image Software Version 4.3 (PerkinElmer) and photon flux was analyzed within regions of interest. *In vivo* data are representative of two independent experiments. Data presented as mean values ± SD. $N = 5$ animals per group.

Preclinical Statistical Analysis

Data were visualized and analyzed using GraphPad Prism software. Data are presented as means ± SD or SEM. For cytotoxicity assays, statistical analysis was performed using a two-way ANOVA with Tukey multiple comparisons. For cytokine release assays, a Student *t* test was conducted as a two-sided unpaired test with a confidence interval of 95%. Statistical analyses of survival were done by log-rank testing. *P* values less than 0.05 were considered significant.

Study Design and Participants

Clinical data through February 8, 2022, are included in this article. This is a phase I study of CNS locoregional adoptive therapy with autologous CD4+ and CD8+ T cells lentivirally transduced to express a B7-H3-specific CAR and EGFRt, delivered by an indwelling catheter in the tumor resection cavity (arm A) or in the ventricular system (arm B) in children and young adults with recurrent or refractory CNS tumors or in the ventricular system (arm C) in children and young adults with DIPG (BrainChild-03; NCT04185038). BrainChild-03 began accrual on November 22, 2019. This study is conducted in accordance with FDA and International Conference on Harmonisation Guidelines for Good Clinical Practice, the Declaration of Helsinki, and applicable institutional review board requirements (study protocol approved by the Seattle Children's Institutional Review Board). All patients or their guardians provided written informed consent in accordance with local regulatory review. Enrollment criteria included: age ≥ 1 and ≤ 26 years (except for the first 3 patients who were ≥ 15 and ≤ 26 and restricted to arms A and B); evidence of refractory or recurrent CNS disease or DIPG/DMG at any time point following completion of standard radiation; ability to tolerate apheresis; presence of a CNS catheter; life expectancy ≥ 8 weeks; Lansky/Karnofsky performance of ≥ 60; defined washout periods from prior therapies; adequate organ function including absolute lymphocyte count (ALC) ≥ 100 cells/μL, absolute neutrophil count ≥ 500 cells/μL, hemoglobin ≥ 9 g/dL, platelets ≥ 100,000/μL, creatinine ≤ upper limit of normal (ULN) for age, total bilirubin < 3× ULN for age or conjugated bilirubin < 2 mg/dL, an oxygen saturation ≥ 90% on room air without dyspnea at rest, adequate neurologic function defined as stable deficits for ≥ 1 week, ≤ 2 antiepileptic agents required to control seizures, and no encephalopathy; negative virology for HIV, hepatitis B, and hepatitis C; and use of highly effective contraception in patients of child-bearing age. Exclusion criteria included: severe cardiac dysfunction; primary immunodeficiency or bone marrow failure syndrome; evidence of impending CNS herniation; presence of > grade 3 dysphagia (for arm C patients); another active malignancy; severe, active infection; active receipt of any anticancer therapy; or pregnancy or breastfeeding.

Enrolled patients underwent leuko-pheresis. CD4+ and CD8+ T cells from apheresis products were bioengineered to express our B7-H3–specific second-generation CAR with an M-spacer length

(Supplementary Fig. S1). BrainChild-03 arm C patients receive locoregional infusions through their CNS catheter on weeks 1 and 3 of each 4-week course, with intrapatient DL escalations in all dose regimens except DR1, during which all doses are delivered at DL1 (Fig. 1). Requirements to receive CAR T-cell infusions included: a CNS catheter in place; ≥ 5 days from surgery; evidence of persistent, evaluable disease; not breastfeeding nor pregnant; meeting defined washout periods from any bridging therapy; adequate organ function defined by specified laboratory values used for eligibility; no encephalopathy or uncontrolled seizure activity; compliance with prescribed antiepileptic drug administration; and no evidence of active severe infection. To receive subsequent infusions, patients additionally were also required to have had no DLT. Beyond course 2, patients were eligible to receive additional infusions at the previous maximum tolerated DL, if the above criteria were met and sufficient CAR T cells were available. Response was assessed following course 2, and subsequent even-numbered courses, using MRI brain and spine and lumbar puncture to evaluate CSF cytology. Correlative studies collections varied by biospecimen and by assigned arm.

Clinical Evaluations

The primary objectives of this study are to assess the feasibility, safety, and tolerability of CNS locoregional adoptive therapy with autologous CD4+ and CD8+ T cells lentivirally transduced to express a B7-H3–specific CAR and EGFRt, delivered by an indwelling catheter in the tumor cavity or ventricular system, in children and young adults with recurrent/refractory CNS tumors and DMG/DIPG. Feasibility is defined as generating sufficient therapeutic product to receive all scheduled doses in courses 1 and 2 at the intended DL per assigned dose regimen after two attempts using a single apheresis product for starting material. Safety and tolerability are determined by data that include history/physical exams, laboratory/radiographic evaluations, and Common Terminology Criteria for Adverse Events (CTCAE v5.0). A DLT is defined as an event that, in the opinion of the investigator, is possibly, probably, or definitely attributable to the CAR T product and that occurs from the time of initial CAR T-cell infusion through 28 days following the final CAR T-cell infusion. A DLT includes all ≥ grade 3 CTCAE v5.0 toxicities except ≥ grade 3 toxicities that are known to be related to CAR T cells, including grade 3 CRS that decreases to ≤ grade 2 within 72 hours; ≥ grade 3 hypotension, fever, and/or chills not controlled with medical intervention that decrease to ≤ grade 2 within 72 hours; ≥ grade 3 activated PTT, fibrinogen, and/or INR that are asymptomatic and resolve within 72 hours; ≥ grade 3 hypoglycemia and/or electrolyte imbalance that are asymptomatic and resolve within 72 hours; ≥ grade 3 nausea and/or vomiting that decrease to ≤ grade 2 with 7 days; grade 3 neurologic symptoms that decrease to ≤ grade 2 with 7 days (for arms A and B); and grade 3 neurologic symptoms that decreases to ≤ grade 2 within 21 days (treatment with dexamethasone and/or bevacizumab is allowed; for arm C). The definition of a DLT also includes any toxicity lasting > 14 days that prevents the patient from meeting criteria for subsequent CAR T-cell infusion in courses 1 or 2. Patients are considered DR escalation-evaluable if they were evaluable for toxicity and were counted as part of a three-patient dose escalation cohort. Our radiologic response criteria use the standard sum of the two longest 2D perpendicular diameters to distinguish: stable disease, progressive disease (>25% increase), partial response (>50% decrease), and complete response (no evaluable or measurable disease).

Cell Product Manufacture

CD4+ and CD8+ T cells were isolated from patient apheresis products using the CliniMACS device (Miltenyi Biotec). A 1:1 mixture of CD4-enriched and CD8-enriched cell fractions were then pooled, suspended in X-Vivo 15 (Lonza) media supplemented with

2% KnockOut SR (Life Technologies), 5 ng/mL rhIL7 (CellGenix), 0.5 ng/mL rhIL15 (CellGenix), and 10 ng/mL rhIL-21 (Miltenyi Biotec), initiated into culture in a G-Rex 100MCS vessel (Wilson-Wolf), and stimulated using CD3/CD28 CTS Dynabeads (Life Technologies). Cell products were then transduced with a GMP-grade SIN (self-inactivating) lentivirus encoding the anti-B7-H3 CAR, the MTX-resistant human DHFR mutein huDHFRdm, and the cell-surface marker EGFRt. On day 3 of culture, 50 nmol/L MTX (Mylan) was added to the culture vessel to select for cells possessing DHFRdm. On day 7 of culture, CD3/CD28 CTS beads were removed from the cell suspension using the Dynamag CTS device. Following 10 to 13 days in culture, patient cells were harvested and washed using the Sepax 2RM device (Cytiva) and resuspended in CryoStor-CS5 (Biolife Solutions) for cryopreservation in CellSeal closed-system vials (Sexton).

CyTOF Analysis

Phenotypic Staining. Cryopreserved CAR T cells were thawed at 37°C for 2 to 3 minutes and washed with complete RPMI + 5 µg/mL DNAse. Cells were transferred to 96-well plates, washed, and resuspended in cytometry buffer (PBS + 0.02% sodium azide + 5% fetal calf serum). Cells were stained with cisplatin at room temperature for 5 minutes and washed twice with cytometry buffer. Following a wash with cytometry buffer, cells were stained with metal-conjugated antibodies against chemokine receptors and incubated at 37°C for 15 minutes in complete RPMI +10% fetal calf serum. Following 2 washes with cytometry buffer, cells were then incubated with PE-conjugated antibody against TCRgd on ice for 15 minutes. Afterward, cells were washed with cytometry buffer and stained with a cocktail of metal-conjugated surface marker antibodies on ice for 30 minutes at concentrations found to be effective in prior antibody tests. Following surface marker staining, cells were washed in 1× intracellular staining permeabilization buffer. Cells were stained with a biotinylated antibody specific against FoxP3 for 15 minutes on ice followed by a wash in 1× intracellular staining permeabilization buffer. Cells were then stained with a cocktail of metal-conjugated antibodies against intracellular transcription factors. After intracellular staining, cells were washed with cytometry buffer and resuspended in PBS + 2% paraformaldehyde.

Stimulation, Staining, and Data Acquisition. Cryopreserved CAR T cells were thawed at 37°C for 2 to 3 minutes and washed with complete RPMI + 5 mg/mL DNAse. For stimulation, 10 × 10⁶ live cells were cultured for 4 hours in 1 mL complete RPMI +10% fetal calf serum + 1× brefeldin A + 50 ng/mL PMA + 1 µg/mL Ionomycin at 37°C in 24-well plates. At the end of the 4-hour stimulation, cells were pipetted vigorously to remove adherent cells from the plate. Cells were transferred to 96-well plates, washed, and resuspended in cytometry buffer (PBS + 0.02% sodium azide + 5% fetal calf serum). Cells were stained with cisplatin at room temperature for 5 minutes and washed twice with cytometry buffer. Following 2 washes with cytometry buffer, cells were incubated with PE-conjugated antibody against TCRγδ on ice for 15 minutes. Afterward, cells were washed with cytometry buffer and stained with a cocktail of metal-conjugated surface marker antibodies on ice for 30 minutes at concentrations found to be effective in prior antibody tests. After surface staining, cells were washed with cytometry buffer and resuspended in PBS + 2% paraformaldehyde. After overnight fixation at 4°C, cells were washed in 1× intracellular staining permeabilization buffer, followed by incubation in 1× intracellular staining permeabilization buffer on ice for 20 minutes. Following incubation, cells were stained with a cocktail of intracellular antibodies for 30 minutes at room temperature. Following intracellular staining, cells were washed 2× with 1× intracellular staining permeabilization buffer and resuspended in 90% fetal bovine serum +10% DMSO to be frozen down in −80°C.

CyTOF Acquisition. Frozen cells were thawed and washed 2× with PBS and barcoded with bromoacetamidobenzyl-EDTA (BABE)-linked metal barcodes to identify individual patient samples as previously described (64). Barcoded cells were washed with 0.5% BSA followed by incubation with a DNA intercalator for 10 minutes on ice. Cells were washed 3× with MilliQ water and resuspended in 10% EQ beads (201078) in MaxPar Cell Acquisition Solution (201240) prior to CyTOF processing.

Data Analysis. The signal of each parameter was normalized based on EQ beads with the Matlab software (https://github.com/nolanlab/bead-normalization/releases/tag/v0.3). Each sample was debarcoded with manual gating on FlowJo. Exported samples or cells of interest were then exported and used for uniform manifold approximation and projection (UMAP) analysis using customized R scripts based on the flowCore (V2.4.0), SingleCellExperiment (V1.14.1), and CATALYST (V1.19.1) R packages (ref. 65; https://www.bioconductor.org/packages/release/bioc/html/flowCore.html, https://www.bioconductor.org/packages/release/bioc/html/CATALYST.html). Downsampling was performed to ensure cell counts are comparable across all samples analyzed within each panel. Cells were first clustered using the clustering algorithm implemented in the CATALYST package, and then manually combined and assigned representative cluster names. Median intensity values were used to construct the cluster heat maps and conduct UMAP analyses.

Antibody Labeling. Purified antibodies used in the phenotype and functional panels are listed in the Excel sheet with the corresponding metal each clone was conjugated to. The antibodies were labeled 100 mg at a time according to instructions provided by Fluidigm Maxpar X8 and MCP9 kits.

The antibodies used for CyTOF include CD4 (Biologend, cat. #300502, RPA-T4), CD8a (BioLegend, cat. #301002, RPA-T8), CD14 (BioLegend, cat. #325602, HCD14), CD19 (BioLegend, cat. #302202, HIB19), CD46 (BioLegend, cat. #318302, HCD56), CD45 (BioLegend, cat. #3089003B, HI30), CLA (BioLegend, cat. #336002, HAE-1f), HLA-DR (BioLegend, cat. #307602, L243), IntegrinBeta7 (BioLegend, cat. #321202, FIB504), TIGIT (Invitrogen, cat. #16950082, MBSA-43), CD69 (BioLegend, cat. #310902, FN50), 2B4 (BioLegend, cat. #329502, C1.7), CD160 (BioLegend, cat. #341202, BY55), CD45RO (BioLegend, cat. #304239, UCHL1), KLRG1 (Thermo Fisher, cat. #16-9488-85, 13F2F12), CD45RA (BioLegend, cat. #304143, HI100), CD27 (Thermo Fisher, cat. #14--0271-82, LG.7F9), Ki-67 (BioLegend, cat. #350502, Ki-67), CD103 (Thermo Fisher, cat. #14-1038-82, B-Ly7), TCRgd-PE + anti-PE (Thermo Fisher, cat. #MHGD04, MHGD04; BioLegend, cat. #408102, PE001), FoxP3-biotin + SAV-155 (Thermo Fisher, 13-4776-82, PCH101), CD3 (BioLegend, cat. #300402, UCHT1), Fas (BioLegend, cat. #305602, DX2), CD161 (BioLegend, cat. #339902, HP-3G10), PD-1 (Thermo Fisher, 14-2799-80, eBioJ105), CD127 (BioLegend, cat. #351302, A019D5), TIM3 (BioLegend, cat. #345002, F38-2E2), LAYN (R&D Systems, MAB26371, 3F7D7E2), CXCR3 (BioLegend, cat. #353702, G025H7), CXCR5 (BioLegend, cat. #552032, RF8B2), CTLA4 (BD Pharmingen, cat. #550405, BNI3), CCR7 (BioLegend, cat. #353202, G043H7), HELIOS (BioLegend, cat. #137202, 22F6), TBET (Thermo Fisher, 14-5825-82, eBio4B10), CCR5 (Bio-Rad, cat. #MCA2175GA, HEK/1/85a), Eomes (Thermo Fisher, cat. #14-4877-82, WD1928), CD39 (BioLegend, cat. #328202, A1), CCR4 (R&D Systems, cat. #MAB1567–100, 205410), CCR6 (BioLegend, cat. #353427, G034E3), CD38 (BioLegend, cat. #303502, HIT2), CD16 (BioLegend, cat. #3209002B, 3G8), Cell-IDTM Intercalator-Ir (Fluidigm, cat. #201192B), CisPlatin live/dead (Sigma-Aldrich, cat. #479306-1G), CD56 (BioLegend, cat. #318202, HCD56), GranzymeK (Santa Cruz Biotechnology, SC-56125), TNFα (BioLegend, cat. #502902, Mab11), IFNγ (BioLegend, cat. #506521, B27), granzyme B (BioLegend, cat. #550558, 2CF/F5), IL6 (BioLegend, cat. #501101, MQ2-13A5), IL3 (BioLegend, cat. #500502, BVD8-3G11), CD25 (BioLegend, cat. #356102, M-A251), IL13 (BioLegend, cat. #501902, JES10-5A2), IL22 (Thermo Fisher, cat. #16-7222-82, IL22JOP), IL2 (BioLegend, cat. #500302, MQ1-17H12), IL8 (BioLegend, cat. #511402, E8N1), Perforin (abcam, cat. #ab47225, B-D48), HLA-DR (BioLegend, cat. #339902, L243),

granzyme A (BioLegend, cat. #557449, CB9), MIP1beta (R&D Systems, cat. #MAB271-100, 24006), IL4 (BioLegend, cat. #500827, MP4-25D2), IL5 (BioLegend, cat. #500902, JES1-39D10), IL10 (BioLegend, cat. #501423, JES3–9D7), GM-CSF (BioLegend, cat. #502315, BVD2–21C11), IL17A (BioLegend, cat. #512331, BL168), IL21 (BioLegend, cat. #513009, 3A3-N2), CD16 (BioLegend, cat. #3209002B), and DNA (Fluidigm, 201192B).

Flow Cytometry for CAR T-cell Detection

Immunophenotyping of surface markers on cells isolated from the CSF correlative specimens was performed using standard staining and flow cytometry techniques, using live/dead viability dye (BD Biosciences) and the following fluorophore-conjugated antihuman monoclonal antibodies: CD3, CD4, CD8a, and CD36 (BD Biosciences). CAR T-cell expression was quantified using cetuximab custom conjugated to allophycocyanin (BD Biosciences) for detection of the EGFRt tag. Cells were also stained with custom-biotinylated trastuzumab and streptavidin (BD Biosciences) for the detection of a HER2 tag not relevant to this trial. CAR T cells were defined as singlets/lymphocytes/viable CD36$^-$/CD3$^+$/EGFRt$^+$HER2$^-$. CD4 and CD8 expression in the CAR$^+$ and CAR$^-$ populations was evaluated. Representative flow gating is in Supplementary Fig. S12. The following antibodies were used for CAR detection in CSF: CD3 (BD Biosciences, cat. #562426, RRID:AB_11152082 or BD Biosciences, cat. #652356, RRID:AB_2868395), CD4 (BD Biosciences, cat. #562658, RRID:AB_2744420), CD8a (BD Biosciences, cat. #560662, RRID:AB_1727513), CD36 (BD Biosciences, cat. #555454, RRID: AB_2291112), cetuximab (Creative Diagnostics, cat. #TAB-003, RRID:AB_2459632) custom conjugated to allophycocyanin by BD Biosciences.

qPCR for CAR T-cell DNA Detection

Assessment of the persistence of CAR T cells in peripheral blood was determined by quantification of the human 5-lipoxygenase-activating protein elongation factor-1 (FLAP-EF1) region of the lentiviral transgene by qPCR. Patient genomic DNA (gDNA) isolated from mononuclear cells from specific timepoints was assessed for *in vivo* persistence by batched analysis. The standard curve for the transcript copy number was established by the amplification of serially diluted plasmid epHIV7. The number of copies of the transgene per nanogram of gDNA input was determined.

Cytokine Profiling

Patient CSF or serum samples were collected and processed by the study site before cryopreservation at −80°C. CSF was collected by either lumbar puncture or ventricular/cavity catheter and maintained at 4°C before and during cell-free supernatant isolation by serial centrifugation. Cells were removed from the CSF sample by spinning at 250 × *g* for 10 minutes followed by a final debris-removal spin at 10,000 × *g* for 10 minutes. Serum was isolated by collection of venous blood in additive-free collection tubes. Following incubation at room temperature for a minimum of 1 hour, collection tubes were centrifuged at 1,000 × *g* for 15 minutes. The resulting supernatant was subsequently centrifuged at 10,000 × *g* for 10 minutes before aliquoting and transfer to storage. Samples were thawed and assessed by batched analysis for select cytokines and chemokines according to the manufacturer's instructions for the 29-plex Human Cytokine/Chemokine Luminex Kit (Millipore, cat. #HCYTMAG60PMX29BK). The Millipore Human Cytokine/Chemokine Panel is a multiplex sandwich capture assay using magnetic antibody-coupled beads that bind cytokine molecules of interest in the CSF or serum sample, biotinylated detection antibody specific for a different epitope on the cytokine, and secondary streptavidin–PE antibody used to label the bead–cytokine complex. All samples and controls are run in duplicate. Samples are analyzed in a flow-based suspension system and the cytokine concentrations in the samples are extrapolated from the general 5-parameter standard curve using Millipore cytokine standard reagent. Heat maps and line plots were generated using R (3.6.3; https://www.r-project.org) with ggplot2 library (3.3.0; ref. 66).

Proteomic Analysis

Serum and CSF (2 × 50 μL aliquots of each sample) were denatured with 200 μL of lysis buffer [25 mmol/L Tris, 7.2 M urea, 1 mmol/L EDTA, 1 mmol/L EGTA, 1% (v/v) Sigma protease inhibitor (#P8340), 1% (v/v) Sigma phosphatase inhibitor cocktail 2 (#P5726), 1% (v/v) Sigma phosphatase inhibitor cocktail 3 (#P0044)]. The plasma was reduced with 30 mmol/L TCEP at 37°C for 30 minutes and alkylated with 50 mmol/L IAM at room temperature for 30 minutes. Urea concentration was diluted 10-fold with 200 mmol/L Tris prior to overnight digestion at 37°C with Lys-C/trypsin using a 1:50 (w/w) enzyme:substrate. Digestions were terminated with formic acid.

The mixture was desalted using Oasis HLB 96-well plates (Waters #WAT058951) and a positive pressure manifold (Waters #186005521) according to the following procedure: wash cartridge with 4 × 400 μL of 50% acetonitrile in 0.1% formic acid, equilibrate with 4 × 400 μL of 0.1% formic acid, load total volume of digest, wash with 4 × 400 μL of 0.1% formic acid, and elute with 3 × 400 μL of 50% acetonitrile in 0.1% formic acid. The eluates were lyophilized and stored at −80°C.

Antibodies were crosslinked on protein G beads (GE Sepharose, #28-9513-79), and peptide enrichment was performed using 1 μg antibody–protein G magnetic beads for each target. Trypsin-digested samples were resuspended in 100 μL 1× PBS + 0.01% CHAPS (pH was adjusted to 7.0 with 10 μL of 1 M Tris, pH 9) and the two digestion aliquots were combined after resuspension to make a total volume of 200 μL. Beads were mixed in the incubation plate, washed twice in 1× PBS buffer + 0.01% CHAPS, washed once in 1/10× PBS + 0.01% CHAPS, and peptides were eluted in 26 μL of 5% acetic acid/3% acetonitrile/50 mmol/L citrate. The elution plate was covered with adhesive foil and frozen at −80°C until analysis. The flow-through was used for subsequent enrichments with assay panels in the same manner as described above.

LC-MS was performed with an Eksigent 425 nanoLC system with a nano autosampler and chipFLEX system (Eksigent Technologies) coupled to a 5500 QTRAP mass spectrometer (SCIEX). Peptides were loaded on a trap chip column (Reprosil C18-AQ, 0.5 mm × 200 μm, SCIEX, #804-00016) at 5 μL/minute for 3 minutes using mobile phase A (0.1% formic acid in water). The LC gradient was delivered at 300 nL/minute and consisted of a linear gradient of mobile phase B (90% acetonitrile and 0.1% formic acid in water) developed from 2–14% B in 1 minute, 14–34% B in 20 minutes, 34–90% B in 2 minutes, and reequilibration at 2% B on a 15 cm × 75 μm chip column (ChromXP 3C18-CL particles, 3 μm, SCIEX, #804-00001). The nano electrospray interface was operated in the positive ion MRM mode. Parameters for declustering potential and collision energy were taken from optimized values in Skyline. Scheduled MRM transitions used a retention time window of 210 seconds and a desired cycle time of 1.5 seconds, enabling sufficient points across a peak for quantification. A minimum of two transitions per peptide, including endogenous and spiked heavy peptides, were recorded for each light and heavy peptide.

MRM data acquired on the 5500 QTRAP were analyzed by Skyline (67, 68). Peak integrations were reviewed manually, and transitions from analyte peptides were confirmed by the same retention times and relative transition areas of the light peptides and heavy stable isotope-labeled peptides. Transitions with detected interferences were not used in the data analysis. Integrated raw peak areas were exported from Skyline and total intensity was calculated using peak area + background. Transitions were summed for each light/heavy pair and peak area ratios were obtained by dividing peak areas of light peptides by that of the corresponding heavy peptides. Concentrations were calculated based on spike levels of heavy peptides. All measurements were filtered by the lower limit of quantification (LLOQ) determined from previous analytical characterization experiments (i.e., all measurements were required to be above the LLOQ).

Data Availability

All requests for raw and analyzed data and materials will be promptly reviewed by the intellectual property office of Seattle Children's Research Institute to verify if the request is subject to any intellectual property or confidentiality obligations. Raw preclinical and clinical data are stored at Seattle Children's with indefinite appropriate backup. Patient-related data not included in the paper were generated as part of clinical trials and may be subject to patient confidentiality. Any data and materials that can be shared will be released via a Material Transfer Agreement.

Authors' Disclosures

K. Seidel reports grants from the NIH during the conduct of the study. J.A. Gustafson reports a patent for a closed-system manufacturing process for CAR T cells pending. A.J. Johnson reports a patent for methods and compositions comprising B7-H3 CARs pending and with royalties paid. J.S. Hauptman reports personal fees from Medtronic and BK Medical outside the submitted work. M.D. Dun reports grants from the National Health and Medical Research Council and RUN DIPG during the conduct of the study, as well as other support from RUN DIPG outside the submitted work. R.J. Orentas reports grants from Miltenyi Biotec outside the submitted work. E.W. Newell reports personal fees and other support from Immunoscape, Neogene Therapeutics, and NanoString Biotechnologies outside the submitted work. J.R. Whiteaker reports personal fees from CellCarta outside the submitted work. A.G. Paulovich reports grants from the NCI and the Aven Foundation during the conduct of the study, as well as personal fees from Precision Assays, LLC., outside the submitted work. J. Gust reports personal fees from Johnson & Johnson outside the submitted work. R.A. Gardner reports other support from Juno Therapeutics, Crispr Therapeutics, Novartis, and Sobi outside the submitted work. M.C. Jensen reports a patent for IL28112921 pending and licensed to Cellevolve, Inc., and subsequent to the performance of the reported data presented in this article, Cellevolve, Inc. has licensed intellectual property pertaining to the B7-H3 CAR from Seattle Children's Research Institute. No disclosures were reported by the other authors.

Disclaimer

The content is solely the responsibility of the authors and does not necessarily represent the official views of the NIH.

Authors' Contributions

N.A. Vitanza: Conceptualization, resources, data curation, formal analysis, supervision, funding acquisition, validation, investigation, methodology, writing–original draft, project administration, writing–review and editing. **A.L. Wilson:** Conceptualization, resources, data curation, formal analysis, supervision, funding acquisition, validation, investigation, methodology, writing–original draft, writing–review and editing. **W. Huang:** Data curation, formal analysis, supervision, funding acquisition, validation, investigation, visualization, methodology, writing–review and editing. **K. Seidel:** Data curation, formal analysis, visualization, writing–review and editing. **C. Brown:** Resources, methodology, writing–review and editing. **J.A. Gustafson:** Resources, data curation, formal analysis, investigation, visualization, writing–review and editing. **J.K. Yokoyama:** Data curation, investigation, writing–review and editing. **A.J. Johnson:** Data curation, investigation, writing–review and editing. **B.A. Baxter:** Investigation, writing–review and editing. **R.W. Koning:** Investigation, writing–review and editing. **A.N. Reid:** Investigation, writing–review and editing. **M. Meechan:** Investigation, writing–review and editing. **M.C. Biery:** Resources, writing–review and editing. **C. Myers:** Resources, writing–review and editing. **S.D. Rawlings-Rhea:** Data curation, formal analysis, visualization, writing–review and editing. **C.M. Albert:** Conceptualization, writing–review and editing. **S.R. Browd:** Conceptualization, writing–review and editing.

J.S. Hauptman: Conceptualization, writing–review and editing. **A. Lee:** Conceptualization, writing–review and editing. **J.G. Ojemann:** Conceptualization, writing–review and editing. **M.E. Berens:** Conceptualization, writing–review and editing. **M.D. Dun:** Conceptualization, writing–review and editing. **J.B. Foster:** Conceptualization, investigation, writing–review and editing. **E.E. Crotty:** Investigation, writing–review and editing. **S.E.S. Leary:** Investigation, writing–review and editing. **B.L. Cole:** Formal analysis, investigation, writing–review and editing. **F.A. Perez:** Conceptualization, formal analysis, investigation, writing–review and editing. **J.N Wright:** Conceptualization, formal analysis, investigation, writing–review and editing. **R.J. Orentas:** Conceptualization, formal analysis, funding acquisition, investigation, visualization, writing–review and editing. **T. Chour:** Conceptualization, formal analysis, supervision, investigation, visualization, writing–review and editing. **E.W. Newell:** Conceptualization, data curation, formal analysis, supervision, investigation, visualization, writing–review and editing. **J.R. Whiteaker:** Data curation, formal analysis, investigation, visualization, writing–review and editing. **L. Zhao:** Conceptualization, data curation, formal analysis, investigation, methodology, writing–original draft, writing–review and editing. **A.G. Paulovich:** Conceptualization, data curation, formal analysis, funding acquisition, investigation, methodology, writing–original draft, writing–review and editing. **N. Pinto:** Conceptualization, investigation, methodology, writing–review and editing. **J. Gust:** Conceptualization, investigation, methodology, writing–review and editing. **R.A. Gardner:** Conceptualization, resources, supervision, funding acquisition, investigation, visualization, methodology, writing–original draft, project administration, writing–review and editing. **M.C. Jensen:** Conceptualization, resources, supervision, funding acquisition, investigation, visualization, methodology, writing–original draft, project administration, writing–review and editing. **J.R. Park:** Conceptualization, supervision, funding acquisition, investigation, visualization, methodology, writing–original draft, project administration, writing–review and editing.

Acknowledgments

Note

Supplementary data for this article are available at Cancer Discovery Online (http://cancerdiscovery.aacrjournals.org/).

REFERENCES

1. Cooney T, Lane A, Bartels U, Bouffet E, Goldman S, Leary SES, et al. Contemporary survival endpoints: an international diffuse intrinsic pontine glioma registry study. Neuro Oncol 2017;19:1279–80.

2. Vitanza NA, Monje M. Diffuse intrinsic pontine glioma: from diagnosis to next-generation clinical trials. Curr Treat Options Neurol 2019;21:37.

3. Louis DN, Perry A, Reifenberger G, von Deimling A, Figarella-Branger D, Cavenee WK, et al. The 2016 World Health Organization classification of tumors of the central nervous system: a summary. Acta Neuropathol 2016;131:803–20.

4. Gardner RA, Finney O, Annesley C, Brakke H, Summers C, Leger K, et al. Intent-to-treat leukemia remission by CD19 CAR T cells of defined formulation and dose in children and young adults. Blood 2017;129:3322–31.

5. Majzner RG, Ramakrishna S, Yeom KW, Patel S, Chinnasamy H, Schultz LM, et al. GD2-CAR T cell therapy for H3K27M-mutated diffuse midline gliomas. Nature 2022;603:934–41.

6. Gregorio A, Corrias MV, Castriconi R, Dondero A, Mosconi M, Gambini C, et al. Small round blue cell tumours: diagnostic and prognostic usefulness of the expression of B7-H3 surface molecule. Histopathology 2008;53:73–80.

7. Zhou Z, Luther N, Ibrahim GM, Hawkins C, Vibhakar R, Handler MH, et al. B7-H3, a potential therapeutic target, is expressed in diffuse intrinsic pontine glioma. J Neurooncol 2013;111:257–64.

8. Lieberman NAP, DeGolier K, Kovar HM, Davis A, Hoglund V, Stevens J, et al. Characterization of the immune microenvironment of diffuse intrinsic pontine glioma: implications for development of immunotherapy. Neuro Oncol 2019;21:83–94.

9. Majzner RG, Theruvath JL, Nellan A, Heitzeneder S, Cui Y, Mount CW, et al. CAR T cells targeting B7-H3, a pan-cancer antigen, demonstrate potent preclinical activity against pediatric solid tumors and brain tumors. Clin Cancer Res 2019;25:2560–74.

10. Vitanza NA, Johnson AJ, Wilson AL, Brown C, Yokoyama JK, Kunkele A, et al. Locoregional infusion of HER2-specific CAR T

11. Du H, Hirabayashi K, Ahn S, Kren NP, Montgomery SA, Wang X, et al. Antitumor responses in the absence of toxicity in solid tumors by targeting B7-H3 via chimeric antigen receptor T cells. Cancer Cell 2019; 35:221–37.

12. Nehama D, Di Ianni N, Musio S, Du H, Patane M, Pollo B, et al. B7-H3-redirected chimeric antigen receptor T cells target glioblastoma and neurospheres. EBioMedicine 2019;47:33–43.

13. Tang X, Zhao S, Zhang Y, Wang Y, Zhang Z, Yang M, et al. B7-H3 as a novel CAR-T therapeutic target for glioblastoma. Mol Ther Oncolytics 2019;14:279–87.

14. Zhang Z, Jiang C, Liu Z, Yang M, Tang X, Wang Y, et al. B7-H3-targeted CAR-T cells exhibit potent antitumor effects on hematologic and solid tumors. Mol Ther Oncolytics 2020;17:180–9.

15. Haydar D, Houke H, Chiang J, Yi Z, Ode Z, Caldwell K, et al. Cell-surface antigen profiling of pediatric brain tumors: B7-H3 is consistently expressed and can be targeted via local or systemic CAR T-cell delivery. Neuro Oncol 2021;23:999–1011.

16. Talbot LJ, Chabot A, Funk A, Nguyen P, Wagner J, Ross A, et al. A novel orthotopic implantation technique for osteosarcoma produces spontaneous metastases and illustrates dose-dependent efficacy of B7-H3-CAR T cells. Front Immunol 2021;12:691741.

17. Loo D, Alderson RF, Chen FZ, Huang L, Zhang W, Gorlatov S, et al. Development of an Fc-enhanced anti-B7-H3 monoclonal antibody with potent antitumor activity. Clin Cancer Res 2012;18:3834–45.

18. Biery MC, Noll A, Myers C, Morris SM, Winter CA, Pakiam F, et al. A protocol for the generation of treatment-naive biopsy-derived diffuse intrinsic pontine glioma and diffuse midline glioma models. J Exp Neurol 2020;1:158–67.

19. Ravanpay AC, Gust J, Johnson AJ, Rolczynski LS, Cecchini M, Chang CA, et al. EGFR806-CAR T cells selectively target a tumor-restricted EGFR epitope in glioblastoma. Oncotarget 2019;10:7080–95.

20. Vitanza NA, Biery MC, Myers C, Ferguson E, Zheng Y, Girard EJ, et al. Optimal therapeutic targeting by HDAC inhibition in biopsy-derived treatment-naive diffuse midline glioma models. Neuro Oncol 2021;23:376–86.

21. Brown CE, Alizadeh D, Starr R, Weng L, Wagner JR, Naranjo A, et al. Regression of glioblastoma after chimeric antigen receptor T-cell therapy. N Engl J Med 2016;375:2561–9.

22. Tang X, Wang Y, Huang J, Zhang Z, Liu F, Xu J, et al. Administration of B7-H3 targeted chimeric antigen receptor-T cells induce regression of glioblastoma. Signal Transduct Target Ther 2021;6:125.

23. Ercikan-Abali EA, Mineishi S, Tong Y, Nakahara S, Waltham MC, Banerjee D, et al. Active site-directed double mutants of dihydrofolate reductase. Cancer Res 1996;56:4142–5.

24. Jonnalagadda M, Brown CE, Chang WC, Ostberg JR, Forman SJ, Jensen MC. Engineering human T cells for resistance to methotrexate and mycophenolate mofetil as an in vivo cell selection strategy. PLoS One 2013;8:e65519.

25. Jonnalagadda M, Brown CE, Chang WC, Ostberg JR, Forman SJ, Jensen MC. Efficient selection of genetically modified human T cells using methotrexate-resistant human dihydrofolate reductase. Gene Ther 2013;20:853–60.

26. Van Oekelen O, Aleman A, Upadhyaya B, Schnakenberg S, Madduri D, Gavane S, et al. Neurocognitive and hypokinetic movement disorder with features of parkinsonism after BCMA-targeting CAR-T cell therapy. Nat Med 2021;27:2099–103.

27. Krishna S, Lowery FJ, Copeland AR, Bahadiroglu E, Mukherjee R, Jia L, et al. Stem-like CD8 T cells mediate response of adoptive cell immunotherapy against human cancer. Science 2020;370:1328–34.

28. Brun V, Masselon C, Garin J, Dupuis A. Isotope dilution strategies for absolute quantitative proteomics. J Proteomics 2009;72:740–9.

29. Neubert H, Shuford CM, Olah TV, Garofolo F, Schultz GA, Jones BR, et al. Protein biomarker quantification by immunoaffinity liquid chromatography-tandem mass spectrometry: current state and future vision. Clin Chem 2020;66:282–301.

30. Netzel BC, Grebe SK, Castro MR, Clark PM, Hoofnagle AN, et al. Thyroglobulin (Tg) testing revisited: Tg assays, TgAb assays, and

correlation of results with clinical outcomes. J Clin Endocrinol Metab 2015;100:E1074–83.

31. Collins CJ, Yi F, Dayuha R, Whiteaker JR, Ochs HD, Freeman A, et al. Multiplexed proteomic analysis for diagnosis and screening of five primary immunodeficiency disorders from dried blood spots. Front Immunol 2020;11:464.

32. Kennedy JJ, Whiteaker JR, Kennedy LC, Bosch DE, Lerch ML, Schoenherr RM, et al. Quantification of human epidermal growth factor receptor 2 by immunopeptide enrichment and targeted mass spectrometry in formalin-fixed paraffin-embedded and frozen breast cancer tissues. Clin Chem 2021;67:1008–18.

33. Kushnir MM, Rockwood AL, Roberts WL, Abraham D, Hoofnagle AN, Meikle AW. Measurement of thyroglobulin by liquid chromatography-tandem mass spectrometry in serum and plasma in the presence of antithyroglobulin autoantibodies. Clin Chem 2013;59:982–90.

34. Do M, Kim H, Yeo I, Lee J, Park IA, Ryu HS, et al. Clinical application of multiple reaction monitoring-mass spectrometry to human epidermal growth factor receptor 2 measurements as a potential diagnostic tool for breast cancer therapy. Clin Chem 2020;66:1339–48.

35. Hembrough T, Thyparambil S, Liao WL, Darfler MM, Abdo J, Bengali KM, et al. Application of selected reaction monitoring for multiplex quantification of clinically validated biomarkers in formalin-fixed, paraffin-embedded tumor tissue. J Mol Diagn 2013;15:454–65.

36. Whiteaker JR, Zhao L, Ivey RG, Sanchez-Bonilla M, Moore HD, Schoenherr RM, et al. Targeted mass spectrometry enables robust quantification of FANCD2 mono-ubiquitination in response to DNA damage. DNA Repair (Amst) 2018;65:47–53.

37. Whiteaker JR, Zhao L, Saul R, Kaczmarczyk JA, Schoenherr RM, Moore HD, et al. A multiplexed mass spectrometry-based assay for robust quantification of phosphosignaling in response to DNA damage. Radiat Res 2018;189:505–18.

38. Abbatiello SE, Schilling B, Mani DR, Zimmerman LJ, Hall SC, MacLean B, et al. Large-scale interlaboratory study to develop, analytically validate and apply highly multiplexed, quantitative peptide assays to measure cancer-relevant proteins in plasma. Mol Cell Proteomics 2015;14:2357–74.

39. Collins CJ, Chang IJ, Jung S, Dayuha R, Whiteaker JR, Segundo GRS, et al. Rapid multiplexed proteomic screening for primary immunodeficiency disorders from dried blood spots. Front Immunol 2018;9:2756.

40. Kennedy JJ, Whiteaker JR, Schoenherr RM, Yan P, Allison K, Shipley M, et al. Optimized protocol for quantitative multiple reaction monitoring-based proteomic analysis of formalin-fixed, paraffin-embedded tissues. J Proteome Res 2016;15:2717–28.

41. Kuhn E, Whiteaker JR, Mani DR, Jackson AM, Zhao L, Pope ME, et al. Interlaboratory evaluation of automated, multiplexed peptide immunoaffinity enrichment coupled to multiple reaction monitoring mass spectrometry for quantifying proteins in plasma. Mol Cell Proteomics 2012;11:M111.013854.

42. Whiteaker JR, Halusa GN, Hoofnagle AN, Sharma V, MacLean B, Yan P, et al. CPTAC assay portal: a repository of targeted proteomic assays. Nat Methods 2014;11:703–4.

43. Whiteaker JR, Lin C, Kennedy J, Hou L, Trute M, Sokal I, et al. A targeted proteomics-based pipeline for verification of biomarkers in plasma. Nat Biotechnol 2011;29:625–34.

44. Whiteaker JR, Zhao L, Lin C, Yan P, Wang P, Paulovich AG. Sequential multiplexed analyte quantification using peptide immunoaffinity enrichment coupled to mass spectrometry. Mol Cell Proteomics 2012; 11:M111.015347.

45. Zhao L, Whiteaker JR, Pope ME, Kuhn E, Jackson A, Anderson NL, et al. Quantification of proteins using peptide immunoaffinity enrichment coupled with mass spectrometry. J Vis Exp 2011;(53):2812.

46. Whiteaker JR, Zhao L, Zhang HY, Feng LC, Piening BD, Anderson L, et al. Antibody-based enrichment of peptides on magnetic beads for mass-spectrometry-based quantification of serum biomarkers. Anal Biochem 2007;362:44–54.

47. Whiteaker JR, Lundeen RA, Zhao L, Schoenherr RM, Burian A, Huang D, et al. Targeted mass spectrometry enables multiplexed quantification of immunomodulatory proteins in clinical biospecimens. Front Immunol 2021;12:765898.

48. Ceppi F, Wilson AL, Annesley C, Kimmerly GR, Summers C, Brand A, et al. Modified manufacturing process modulates CD19CAR T-cell engraftment fitness and leukemia-free survival in pediatric and young adult subjects. Cancer Immunol Res 2022;10:856–70.

49. Gruver AL, Hudson LL, Sempowski GD. Immunosenescence of ageing. J Pathol 2007;211:144–56.

50. Dorshkind K, Swain S. Age-associated declines in immune system development and function: causes, consequences, and reversal. Curr Opin Immunol 2009;21:404–7.

51. Tang X, Liu F, Liu Z, Cao Y, Zhang Z, Wang Y, et al. Bioactivity and safety of B7-H3-targeted chimeric antigen receptor T cells against anaplastic meningioma. Clin Transl Immunology 2020;9:e1137.

52. Guedan S, Posey AD Jr, Shaw C, Wing A, Da T, Patel PR, et al. Enhancing CAR T cell persistence through ICOS and 4-1BB costimulation. JCI Insight 2018;3:e96976.

53. Jin L, Tao H, Karachi A, Long Y, Hou AY, Na M, et al. CXCR1- or CXCR2-modified CAR T cells co-opt IL-8 for maximal antitumor efficacy in solid tumors. Nat Commun 2019;10:4016.

54. Jain MD, Zhao H, Wang X, Atkins R, Menges M, Reid K, et al. Tumor interferon signaling and suppressive myeloid cells are associated with CAR T-cell failure in large B-cell lymphoma. Blood 2021;137:2621–33.

55. Theruvath J, Sotillo E, Mount CW, Graef CM, Delaidelli A, Heitzeneder S, et al. Locoregionally administered B7-H3-targeted CAR T cells for treatment of atypical teratoid/rhabdoid tumors. Nat Med 2020;26:712–9.

56. Donovan LK, Delaidelli A, Joseph SK, Bielamowicz K, Fousek K, Holgado BL, et al. Locoregional delivery of CAR T cells to the cerebrospinal fluid for treatment of metastatic medulloblastoma and ependymoma. Nat Med 2020;26:720–31.

57. Gallego Perez-Larraya J, Garcia-Moure M, Labiano S, Patino-Garcia A, Dobbs J, Gonzalez-Huarriz M, et al. Oncolytic DNX-2401 virus for pediatric diffuse intrinsic pontine glioma. N Engl J Med 2022;386:2471–81.

58. Hudecek M, Lupo-Stanghellini MT, Kosasih PL, Sommermeyer D, Jensen MC, Rader C, et al. Receptor affinity and extracellular domain modifications affect tumor recognition by ROR1-specific chimeric antigen receptor T cells. Clin Cancer Res 2013;19:3153–64.

59. Kunkele A, Johnson AJ, Rolczynski LS, Chang CA, Hoglund V, Kelly-Spratt KS, et al. Functional tuning of CARs reveals signaling threshold above which CD8+ CTL antitumor potency is attenuated due to cell Fas-FasL-dependent AICD. Cancer Immunol Res 2015;3:368–79.

60. Wang X, Chang WC, Wong CW, Colcher D, Sherman M, Ostberg JR, et al. A transgene-encoded cell surface polypeptide for selection, in vivo tracking, and ablation of engineered cells. Blood 2011;118:1255–63.

61. Guedan S, Calderon H, Posey AD Jr, Maus MV. Engineering and design of chimeric antigen receptors. Mol Ther Methods Clin Dev 2019;12:145–56.

62. Watanabe N, Bajgain P, Sukumaran S, Ansari S, Heslop HE, Rooney CM, et al. Fine-tuning the CAR spacer improves T-cell potency. Oncoimmunology 2016;5:e1253656.

63. Erskine CL, Henle AM, Knutson KL. Determining optimal cytotoxic activity of human Her2neu specific CD8 T cells by comparing the Cr51 release assay to the xCELLigence system. J Vis Exp 2012;(66)e3683.

64. Mrdjen D, Pavlovic A, Hartmann FJ, Schreiner B, Utz SG, Leung BP, et al. High-dimensional single-cell mapping of central nervous system immune cells reveals distinct myeloid subsets in health, aging, and disease. Immunity 2018;48:380–95.

65. Amezquita RA, Lun ATL, Becht E, Carey VJ, Carpp LN, Geistlinger L, et al. Orchestrating single-cell analysis with Bioconductor. Nat Methods 2020;17:137–45.

66. Wickham H. ggplot2: Elegant graphics for data analysis. New York: Springer; 2016.

67. MacLean B, Tomazela DM, Shulman N, Chambers M, Finney GL, Frewen B, et al. Skyline: an open source document editor for creating and analyzing targeted proteomics experiments. Bioinformatics 2010;26:966–8.

68. Pino LK, Searle BC, Bollinger JG, Nunn B, MacLean B, MacCoss MJ. The Skyline ecosystem: informatics for quantitative mass spectrometry proteomics. Mass Spectrom Rev 2020;39:229–44.